COMPUTATIONAL MODELING OF ALLOY NANOPARTICLE STABILITY

by

Zihao Yan

B.S. Chemical Engineering, University of California at Berkeley, 2014

Submitted to the Graduate Faculty of

Swanson School of Engineering in partial fulfillment

of the requirements for the degree of

Master of Science

University of Pittsburgh

2018

UNIVERSITY OF PITTSBURGH

SWANSON SCHOOL OF ENGINEERING

This thesis was presented

by

Zihao Yan

It was defended on

May 11, 2018

and approved by

Goetz Veser, Ph.D., Nickolas A. DeCecco Professor
Department of Chemical and Petroleum Engineering

Guofeng Wang, Ph.D., Associate Professor
Department of Mechanical Engineering and Materials Science

Thesis Advisor: Giannis Mpourmpakis, Assistant Professor
Department of Chemical and Petroleum Engineering

COMPUTATIONAL MODELING OF ALLOY NANOPARTICLE STABILITY

Zihao Yan, M.S.

University of Pittsburgh, 2018

Metal nanoparticles (MNPs) are an exciting class of materials, finding applications in optical devices, electronics, drug delivery and chemical catalysis. Despite numerous applications, understanding of MNP stability is somewhat limited. First principles methods such as Density Functional Theory and semi-empirical models such as embedded atom model either suffer of high computational cost or inaccuracy. Herein, we introduce a bond-centric (BC) model to describe the cohesive energy of monometallic and bimetallic nanoparticles with arbitrary morphologies and chemical composition. We apply our BC model on a range of mono- and bi-metallic nanoparticles (nanoalloys) and demonstrate a great agreement with Density Functional Theory calculations. Moreover, we show our BC model effectively captures mixing behavior of nanoalloys through excess energy analysis. Additionally, we apply our BC model to perform energetic screening on a recently-published 23196-atom FePt nanoalloy and its homotops, offering insights of both segregation and chemical ordering behavior. The screening we performed is beyond reach of DFT because of the extremely large MNP size and number of nanoalloy conformations. Our findings are in agreement with literature. Therefore, our BC model is shown to be a powerful and computationally inexpensive tool to calculate energetics of almost any MNP, thus significantly accelerating MNP design.

TABLE OF CONTENTS

LIST OF FIGURES

PREFACE

I am very grateful to my thesis advisor, Dr. Giannis Mpoumpakis, for his guidance and efforts to train me into a researcher. With his mentoring and support, I am glad to see how much I improved during my two years as a M.S. student. I am also very grateful to my lab mate, tutor and friend Michael Taylor. He gave me priceless help in both science and life. Moreover, I want to express my gratitude to everyone in my group for all their help throughout these years. It's a privilege working with you! In addition, I would like to thank the University of Pittsburgh and the Chemical Engineering Department for giving me comprehensive education and valuable research opportunities. Last but not least, I am very grateful to my family and friends for their tremendous mental and physical support. It was the support of all these respectable people helping finish this thesis project and I hope that this work will help other researchers in the field.

1.0 INTRODUCTION

As a burgeoning technology, metal nanoparticles (MNPs) have tremendous application in a wide range of fields: from electronics and optical devices,[4] to biological detectors and drug delivery,[5] to chemical catalysis.[6-7] MNPs are promising in these applications in large part because of their unique properties (i.e. optical,[8] electronic,[9-10] magnetic[11] and adsorption behavior[12-14]) that differ from both the atomic and bulk size extremes. These properties are dictated by MNP morphology[12] (i.e. size[15] and shape[16-17]) and composition.[12, 18] Compared with monometallic MNPs, bimetallic MNPs (nanoalloys) have more tunable properties[19-20] achieved by shifts in composition (both elements and elemental ratios) and are more adaptable for application in broad areas.[6] Beyond composition, chemical ordering at the atomic level determines nanoalloy properties in magnetic[21] and catalytic applications.[22] Chemical ordering contributes significant diversity of nanoalloys and increases the amount of work to comprehensively study nanoalloy properties. For example, a single 25-atom nanoalloy structure with no identical positions comprised of 15 Au and 10 Ag atoms has 3268760 distinct homotops. Beyond desirable properties, MNPs must be stable enough to be synthesized and to survive any potential application. Therefore, a deep understanding of the relationship between MNP stability and factors including morphology, composition and chemical ordering is essential for engineering MNPs with tailored properties for specific applications. An important energetic factor that can capture structure-dependent stability is

Cohesive Energy (CE) defined as difference between energy of a MNP (E_{MNP}) and summation of energy of individual atoms:

$$CE = \frac{E_{MNP} - \sum_1^n E_i}{n} \quad (1\text{-}1)$$

where E_i is energy of an individual atom and n is the total number of atoms inside MNP. From equation 1-1, we can see a MNP structure with more negative CE indicates lower energy (E_{MNP}) of the MNP. The value of E_{MNP} and thus of CE is affected by all the factors (morphology, composition, and chemical ordering) impacting MNP's properties described earlier. Therefore, CE is a good descriptor of MNP stability and indicator of how these structural and compositional factors affect MNP stability.

Several theories or models have been developed in literature to predict CE and help understand MNP stability including Embedded-atom method (EAM),[23-24] Density Functional Theory (DFT)[25-26], Tight Binding Method[27-28] and Square-root bond cutting (SRB) model.[29] In particular, DFT was used as the calibrator of our work and SRB model (derived from Tight Binding Model) is the basis of our new model. Detailed introduction of DFT, Tight Binding, and SRB models are presented in the following sections.

1.1 DENSITY FUNCTIONAL THEORY

Density Functional Theory (DFT) developed by Walter Kohn[30] is a well-established approach to describe energies in many-body systems accurately and efficiently which are analytically unsolvable by traditional approach of solving Schrodinger equation.[25] DFT has been widely used in the field of condensed matter physics and chemistry.[31-32]

Different from wave function-based approaches e.g. Schrodinger equation,[33] DFT assumes solving for the electron density distribution is capable of fully describing electronic structure. The underlying theorem of DFT is the Hohenberg-Kohn (H-K) theorem. According to H-K theorem, the ground state energy is a unique functional of the ground state electron density and the electron density corresponding to the solution of Schrodinger equation is the electron density that minimizes the overall functional energy. The electron density for a N-particle system is

$$\rho(r) = \sum_i^N |\varphi_i(r)|^2. \tag{1.2}$$

where $\varphi_i(r)$ is Kohn-Sham (KS) orbital. In DFT, the ground-state energy ($E[\rho]$) is given by the Kohn-Sham equation (DFT equivalent of the Schrodinger equation) as:

$$E[\rho] = T_s[\rho] + \int dr\, v_{ext}(r)\rho(r) + E_H[\rho] + E_{XC}[\rho] \tag{1.3}$$

Where $T_s[\rho]$ is the KS kinetic energy which is a sum of a functional of the molecular orbitals, v_{ext} is the external potential representing the interaction between an electron and the nuclei, E_H is the Hartree potential which represents the interaction between an electron with electron density defined by other electrons and E_{XC} is the exchange-correlation energy. E_{XC} is comprised of an exchange energy term describing the energy released when two or more electrons with same spin exchange their positions and a correlation energy term describing the influence on an electron's movement by all other electrons. The E_{XC} is the only mathematically undefined term in KS equation for which effective approximations are required. The first approximation widely used was the local-density approximation (LDA) which sets exchange-correlation energy at each point to be the known exchange-correlation energy from uniform electron gas at the same density.[30] The current widely used assumption is the generalized gradient approximation, known as GGA, considers both local electron density and its gradient.[34-35] In literature, use of GGA instead of LDA

on small molecules reduced errors by factors of 3-5.[25] In addition, GGA has been successfully applied to investigate properties of MNPs.[36-37] Some commonly-used GGA functionals include the Perdew-Wang (PW91) and Perdew-Burke-Ernzerhof (PBE) functionals.

In the present thesis, we used PBE exchange-correlation functional as it has been used in literature to accurately model energetics for systems ranging from molecules to solids.[38] In particular, PBE has been widely used to calculate energetics of MNPs.[39-40] In general, we consider DFT results to be accurate predictions of experimental results and thus used DFT as the calibrator to test the accuracy of other models.

Despite its accuracy, DFT has its disadvantages. First, DFT becomes computationally intractable at even moderate MNP sizes (~1-3 nm diameter MNPs)[41] and is largely prohibitively expensive in studying nanoalloys due to their near infinite homotops.[42-43] Therefore, other methods are needed to develop an accurate but inexpensive method for working on nanoalloys of arbitrary size and composition to accelerate nanoalloy discovery and design.

1.2 FROM TIGHT-BINDING METHOD TO SQUARE-ROOT BOND CUTTING MODEL

The tight-binding (TB) method[44] is a very simple scheme compared to DFT to describe cohesive properties from atomic and electronic structures. According to TB model, the cohesive energy of an atom i is comprised of an attractive term represented by effective band energy (electronic binding energy) and a short-range repulsive interaction term:

$$CE_i = E_i^B + E_i^R \tag{1.4}$$

where E_i^B represents the binding energy which is also called band energy because when transition metal atoms are placed into a solid, the atomic d electron energy of atoms spreads into a band. E_i^R represents repulsive energy (known as Born-Mayer potential) which describes core-core interactions as two atoms approach.[45] As E_i^R is much smaller than the band energy term, it can be neglected for calculating cohesion at equilibrium distance. To evaluate the band energy, Tomanek et al. proposed the second-moment approximation of the tight-binding scheme (TB-SMA).[29, 46] The TB-SMA scheme assumes a rectangular shape of electronic band and band energy is thus proportional to the band width.[27] Note that when local band occupancies stay the same, cohesive energy is purely proportional to W_i:[29]

$$CE_i \cong E_i^B \propto W_i \tag{1.5}$$

The band width, W_i is proportional to the square root of the second moment, $\sqrt{\mu_2}$ (mathematically proved by Ackland Et al. in 1988).[47] The second moment, μ_2 of electron density of states (DOS) is defined as the contribution of all closed electron paths of two steps to electron DOS. Applying the linear combination of atomic orbitals (LCAO) assumption, μ_2 can be written as a linear combination of squares of hopping integrals describing electron paths of two steps (jumping from a given site to the other site and jumping back) as:

$$\mu_2 = CN(dd\sigma^2 + 2dd\pi^2 + 2dd\delta^2) \tag{1.6}$$

where CN is the coordination number representing number of the first neighbors of an atom and σ , π and δ are magnetic quantum number of basic orbitals. From equation (1.6), we can see μ_2 is directly proportional to CN. Note that TB-SMA can move on to create an expression of band energy in terms of a series of potential parameters[27] which require heavy experimental data to be evaluated. Tomanek[29] avoided such problem by dividing CE over the bulk cohesive energy and all other terms are cancel out except the CNs:

$$\frac{CE_i}{CE_{bulk,i}} = \frac{W_i}{W_{i,bulk}} = \frac{\sqrt{\mu_{2,i}}}{\sqrt{\mu_{2,bulk}}} = \frac{\sqrt{CN_i}}{\sqrt{CB_i}} \quad (1.7)$$

where CB_i is the bulk coordination number which is 12 for fcc/hcp and 8 for bcc structures. Cohesive energy of an atom can thus be expressed in terms of bulk cohesive energy and coordination numbers:

$$CE_i = CE_{bulk,i}\sqrt{\frac{CN_i}{CB_i}}. \quad (1.8)$$

Note that effective coordination number (ECN) when interaction from second neighbors are considered for more accurate predictions:

$$ECN = CN + \alpha CN^1. \quad (1.9)$$

where CN^1 is the coordination number of atom i's first neighbor and α is a constant coefficient which is 0.08 (0.4) for fcc (bcc) metals. However, we can just use CN instead of ECN for fcc MNPs as the second neighbor correction term is very small. The cohesive energy of a metal nanoparticle with n atoms is thus given by:

$$CE_{MNP} = \frac{\sum_1^n CE_i}{n} = \frac{1}{n}\sum_1^n CE_{bulk,i}\sqrt{\frac{CN_i}{CB_i}}. \quad (1.10)$$

We call equation 1.10 the square-root bond cutting (SRB) model. The SRB model is a very simple but accurate model to describe cohesive energy and requires only bulk CE values which can be found in literature. Note that accurate determination of CN is essential for SRB model. We thus created a code which accurately assign CN to each atom that is included in the Appendix.

Compared with electron-density centric methods (EAM and DFT), the atom-centric SRB model is computationally very inexpensive. $CE_{bulk,i}$ are the only experimental values needed for the SRB model and $CE_{bulk,i}$ of all elements can be found tabulated in literature.[48] Applying the SRB model, CEs of large number of MNPs with arbitrary size and morphology is possible.

In this thesis, we tested the accuracy of SRB model on Au, Ag, Cu, and Zr MNPs with a wide range of sizes and shapes. We also tested SRB model's sensitivity on morphology. Due to the promising results, we choose SRB model as a starting point to create a new model for addressing bimetallic energetics. As an atom-centric model, the SRB model cannot capture most chemical ordering effects in bimetallic MNPs. Therefore, based on the SRB model we proposed an improved model which can calculate CE of MNPs with arbitrary composition and morphology. Due to its bond-centric scheme, we call our new model the bond-centric (BC) model.

2.0 METHODOLOGY

Density Functional Theory (DFT) calculations were performed using PBE exchange-correlation functional[49] combined with the DZVP basis set[50] as implemented in the CP2K package.[51] PBE is ubiquitous in evaluating energetics of transition metals.[39-40] Geometry relaxations were performed via quasi-Newton-Raphson minimization to determine total electronic energies of Au/Ag/Cu/Zr MNPs and CuAg/CuZr nanoalloys. During geometry relaxation, the energy cutoff of the basis set was 500 Rydberg and the force cutoff was 0.0004 Ha/Bohr. We used 40X40X40 Angstroms unit cell with all structures positioned in the center of the box. Examples of CP2K input files (.inp, .xyz) are attached in the Appendix A. MNPs and nanoalloys with Icosahedral and Octahedral shapes were created using Atomic Simulation Environment (ASE). MNPs and nanoalloys with pyramid and cubic shapes were created using Materials Studio. Equation (1-1) was used to calculate CEs based on DFT-calculated MNP energies and single-atom energies. We also calculated excess energy (EE), another important energetic factor describing nanoalloy stability. The EE describes the tendency of forming a nanoalloy rather than two separated monometallic MNPs and the EE of nanoalloy A_xB_y is calculated as:

$$EE = CE_{A_xB_y} - \frac{x}{x+y}CE_{A_{x+y}} - \frac{y}{x+y}CE_{B_{x+y}} \quad (2\text{-}1)$$

Where $CE_{A_xB_y}$ is the cohesive energy of the alloy, $CE_{A_{x+y}}$ and $CE_{B_{x+y}}$ are the cohesive energies of pure A and B MNPs with x+y atoms. The derivation of equation (2-1) is attached in Appendix B.

To aid with implementation and calculation of the SRB and BC models we created several Python codes. First, we created a code able to assign CNs to each atom in arbitrary MNPs and nanoalloys. Second, we created codes to calculate CE applying SRB model and BC model. Third, we created homotop-generating code which generates an arbitrary amount of homotops of the FePt nanoalloy we studied for this thesis and calculates their CE and EE at the same time. These codes are outlined below and are included in the Appendix.

2.1 BOND-CENTRIC MODEL

Herein we introduce our bond-centric (BC) model which moves beyond the atomic-centric SRB model and can capture alloy effects. The design of BC model is based on the fact that CE can be expressed by the summation of bond energies (BE) of all the chemical bonds inside the particle:

$$CE_{MNP} = \frac{\sum_1^m BE_{ij}}{n} \tag{2-2}$$

where BE_{ij} represents the bond energy stored between atoms i and j (also known as bond-disassociation energy), m is the total number of bonds in the MNP and n is the total number of atoms. Each BE_{ij} can be expressed by a sum of half-bond energies (HBE) from the two atoms i and j while HBE equals to the atom's CE divided by its CN (number of bonds):

$$BE_{ij} = HBE_i + HBE_j = \frac{CE_i}{CN_i} + \frac{CE_j}{CN_j} \tag{2-3}$$

where HBE_i and HBE_j are HBE of atoms i and j respectively. Equation (2-3) stands correct so long as atom i and j are same element so that HBEs from each atom contribute equally to BE_{ij}. Note that in this condition (monometallic MNPs), we will get mathematically the same expression as SRB model when we combine equation (2-2) and (2-3) together. However, for heterolytic bonds

in nanoalloys, the assumption of equal contributions may not hold, as one element tends to be more favored than the other. Therefore, we introduce weight factors γ_i and γ_j to incorporate element-dependent bond weighting:

$$BE_{ij} = \gamma_i HBE_i + \gamma_j HBE_j \tag{2-4}$$

where γ_i and γ_j are the wright factors for atoms i and j. Values of γ_i and γ_j are calculated based on literature values of molecular dimer bond disassociation energies (BDE). For a heterolytic dimer bond containing elements A and B, the weighting factors γ_A and γ_B are calculated from the following equations:

$$X * \gamma_A + Y * \gamma_B = 2 * Z \tag{2-5}$$

$$\gamma_A + \gamma_B = 2 \tag{2-6}$$

where X is the experimental or theoretical BDE of an A_2 bond, Y the B_2 BDE and Z the AB BDE. We set $\gamma_A + \gamma_B = 2$ because we are summing up 2 half-bonds to calculate BE_{ij}. Note that γ_A=γ_B=1 when A and B are the same element (for homolytic bonds). Also, we have 2*Z on the right side of equation (2-5) to follow conservation of mass. Combining equation (2-2), (2-3) and (2-4), we have the complete form of BC model as:

$$CE_{MNP} = \frac{\sum_1^m \gamma_i \frac{CE_{bulk,i}}{CN_i}\sqrt{\frac{CN_i}{CB_i}} + \gamma_j \frac{CE_{bulk,j}}{CN_j}\sqrt{\frac{CN_j}{CB_j}}}{n} \tag{2-7}$$

3.0 RESULTS AND DISCUSSION

The results presented in this section have been taken in part from our publication Yan Z. et al., Nano Lett., 2018, 18, 2696–2704.[52]

In this chapter, we first presented theoretical basis and logic of our codes which are included in the Appendix and tested the SRB model performance over a series of monometallic MNPs including Au, Ag, Cu and Zr with various morphology. We then assessed the power of SRB model to capture shape differences on 55-atom MNPs with various shapes. Based on these results, we claim the SRB model is able to capture stability behavior of MNPs with a wide range of sizes and shapes.

Next, we tested performance of the BC model compared to SRB model against DFT calculations on CuAg, CuZr, CuAu, and AuAg nanoalloys of different size, shape and composition. In addition to CE, we tested BC model's performance on EE prediction against DFT results. We thus confirm BC model's advantage over SRB model on prediction of nanoalloys and summarize the BC model limitations.

To further explore the power of BC model, we applied the BC model on an experimentally-synthesized 23196-atoms FePt nanoalloy and its homotops (which is well beyond the reach of DFT). For comparison with DFT, we used the BC model to screen over 20,000 homotops in minutes. We perform a comprehensive analysis on the chemical ordering effect over the CE and EE of nanoalloys and get results in agreement with experimental literature. Last, we discuss the

applicability and limitations of BC model. We also suggest ways to overcome some of these limitations.

In conclusion, we have performed a comprehensive assessment on the BC model and proved it to be a powerful tool to analyze stability behaviors of nanoalloys with respect to size, shape, composition, and chemical ordering effects.

3.1 CODING

The purpose of this section is to give an introduction on the theoretical basis and logic of our Python codes. Here, we use the automatic CN determination code as an example because this code requires theoretical basis regarding definitions of first neighbors and relatively complicated logic. This code is the corner stone to apply both SRB model and BC model. The CE calculator and homotop generator are pure Python codes doing calculation and atom assignment jobs without requirement of theoretical basis. As all the codes have been published on Github, anyone can download the codes and check the programing details.

The CN-determination code automatically assigns CN to each atom in MNPs with arbitrary morphology and composition. Our code applies Van der Waals radius[53] (VDWR) as a starting place for determining neighbors of a given atom. Two atoms are defined as direct neighbors when the distance between them are shorter than the sum of their VDWR. The CN of a given atom is defined as the number of neighbors of an atom. Since the initial guess of the VDWR radii is usually longer than the corresponding chemical bond, a scaling factor is introduced to 1: prevent over-estimation of CNs and to 2: maintain a consistent and systematic approach to reduce the VDWR of the atoms in a MNP/alloy structure. Starting from a higher value, the code will automatically

cut down the scaling factor of the atom type that has the most exceptions by a step of 0.001 time and recalculate the CNs until either no atom in the MNP has CN larger than 12 (the maximum CN possible in fcc structure), or a minimum number of exceptions are reached for an amorphous alloy MNP. For alloy MNPs, if the ratio of the VDWR between two elements (VDWR ratio) is greater than 1.1, the MNP is treated as amorphous. Exceptions are added (i.e. allowances for atoms with CN>12) for amorphous MNPs, since we found that slightly overestimating CN has a minimal impact on the bond-centric (BC) model relative to underestimations of CNs. This is because underestimation affects mostly the surface atoms while over estimation affects mostly bulk atoms, while surface atoms dominate in small-sized MNPs (Figure S1). In addition, mathematically, an overestimation of an atom's CN (e.g. from 12 to 13) has a less effect on the CE calculation than underestimation of another atom's CN (e.g. from 5 to 4), as our model is adding up square roots of the CNs (ie. ($\left|\sqrt{13}-\sqrt{12}\right| < \left|\sqrt{4}-\sqrt{5}\right|$). For pure MNPs, the initial scaling factor is 0.875 instead of 1 to prevent over-estimation, and to maintain a consistent VDWR still exists because no atoms in monometallic MNP are prone to be over-coordinated (CN>12), although checks to ensure no CNs>13 are still performed. For bimetallic MNPs, the initial scaling factor is 1 and more complicated mechanism is applied regarding how to cut down the scaling factor. The details of cutting and programming logic are annotated in the released code.

3.2 MONOMETALLIC METAL NANOPARTICLES

We tested SRB model on monometallic MNPs diverse in metals (Au, Ag, Cu, Zr), size (19-172 atoms), and shape (Cubic (Cb), Decahedral (Dh), Icosahedral (Ih), Octahedral (Oh)) as highlighted in Figure 1. We selected Au/Ag because of their ubiquity in MNP literature[4] and Cu/Zr

due to their promise in catalysis.[54] Moreover, all these metals have close-packed structures (fcc for Au/Ag/Cu, hcp for Zr) indicating they are theoretically stable in the same MNP structures. The shapes we selected were highly-symmetric representing lower-energy structures.

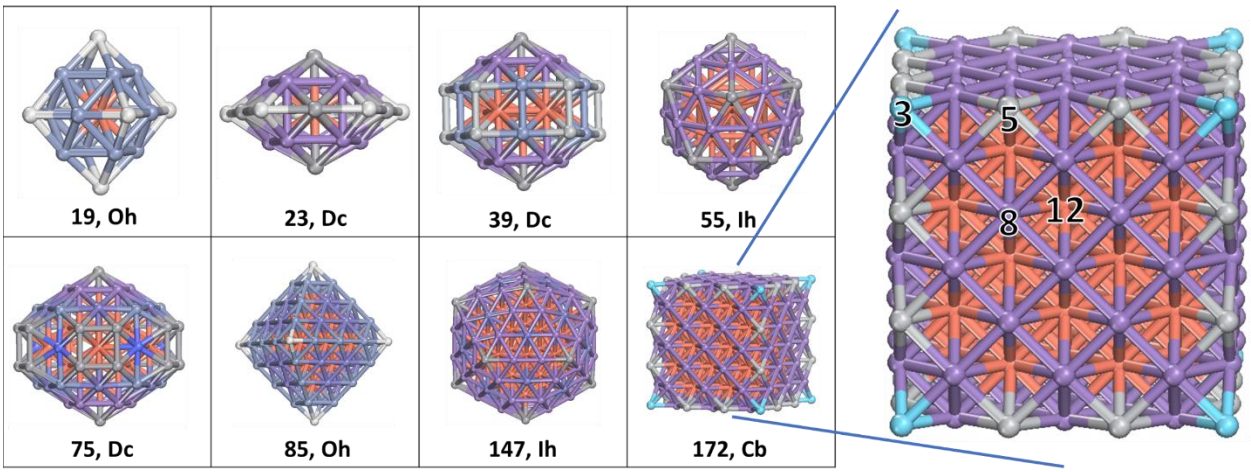

Figure 1. Metal nanoparticles (MNPs) representing different sizes and shapes (morphologies; Oh=Octahedron, Dc=Decahedron, Ih=Icosahedron, Cb=Cubic). Atoms with different CNs are represented with different colors (color ranges from light blue for CN=3 atoms to orange for CN=12 atoms), as shown on the expanded 172, Cb MNP.

To directly compare DFT and the SRB model, we used DFT-calculated value of CE_{bulk} ($CE_{bulk,DFT}$) in the SRB model. $CE_{bulk,DFT}$ was estimated using a simple $n^{-1/3}$ vs. CE relation as presented in Figure 2. The $CE_{bulk,DFT}$ we calculated is also in good agreement with literature values calculated for PBE DFT[55](except Zr as literature value refers to hcp Zr). Note that SRB inherits some limitations of the DFT due to the use of $CE_{bulk,DFT}$ values. For example, as Figure 2 shows, DFT underestimatesCE_{bulk} of Au and Ag relative to experimental CE_{bulk}values.[48] We will discuss how this underestimation affects the prediction of both SRB and BC model in the later section.

a

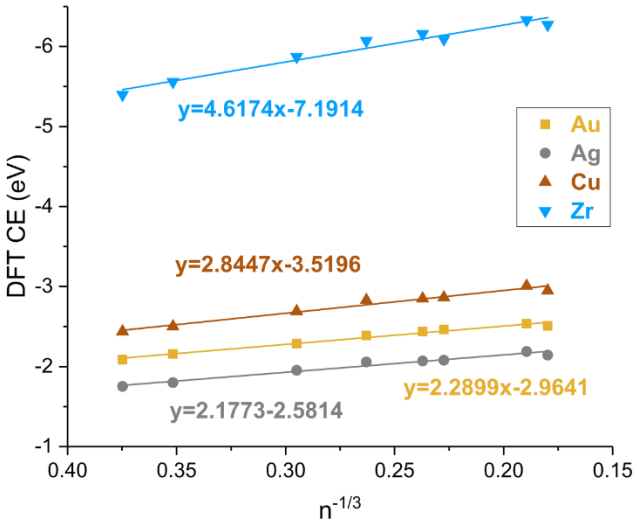

b

CE_{bulk}	DFT Calculation	Experimental Value	Reference DFT Value
Cu	-3.52 eV	-3.49 eV	-3.48 eV
Ag	-2.58 eV	-2.95 eV	-2.49 eV
Au	-2.96 eV	-3.81 eV	-3.99 eV
Zr	-7.19 eV	-6.25 eV	-6.16 eV

Figure 2. (a) CE_{bulk} calculations from DFT results for Au, Ag, Cu and Zr (limit of y-axis intercepts). Structures used to calculate CE_{bulk} are those shown in Figure 1. (b) Table of CE_{bulk} values from both *our* DFT calculations and from literature *(experimental[48] and periodic DFT[55])*.

Parity between the cohesive energy (CE) of the SRB model and accurate DFT calculations on the structures shown in Figure 1 is presented in Figure 3. Note that the equations of fit in Figure 3 were forced to intercept at the origin to capture the physical limits of CE (given the fact that a single atom has CE=0). We note in Figure 3 that the SRB model predicts CE of all MNPs within 5% error against DFT calculations with high R^2 values and gives identical trends as DFT for all metals. The SRB model predicts generally higher CEs for larger MNPs on the same metal and a CE trend based on metal types: i.e. Zr>Cu>Au>Ag (identical to DFT predicted CE_{bulk} trend in Figure 2b). These trends indicate that SRB model captures the MNP CE dependence on the size and metal types. The deviation between the SRB model and DFT calculations is caused by multiple factors including assumptions Tomanek made when deriving SRB model (E_R, rectangular-shape electronic band, LCAO) and strain effects. Strain is caused when atoms (especially surface atoms) deviate from the perfect lattice positions after relaxation and this effect will cause higher energy

of MNPs. Strain effects can be captured by DFT but not by the SRB model. We also notice that unlike the other three metals, the CEs of Zr MNPs are underestimated, likely because Zr is an hcp metal. In hcp metals, the (0001) plane intralayer bond lengths are not equivalent with interlayer bond lengths, meaning a bulk hcp atom more accurately has 6 nearest neighbors and another 6 near-nearest neighbors.[56] Thus, the true CB value for hcp metals is likely less than 12 and if this value is plugged into SRB model, values of CEs for Zr will be shifted higher in Figure 3. Another plausible explanation is that the squire-root approximation works best for metals with half-filled d bands,[57] though we are expanding this approximation to all transition metals. This assumption at least partially explains the observation that elements with almost-filled d bands (Au,Ag,Cu) locate above the parity line while Zr whose d band is almost empty locates below the parity line. Visually, Ag and Zr are in the same row of element table, having same distance from half-filled d-band elements and they both have around 4% error from the parity line. However, further tests on elements between Ag and Zr (like Ni) are required to substantiate this explanation. We did not include factors like nanoscale metal- and size-dependent strain and hcp interlayer stacking effects to preserve the simplicity of SRB model.

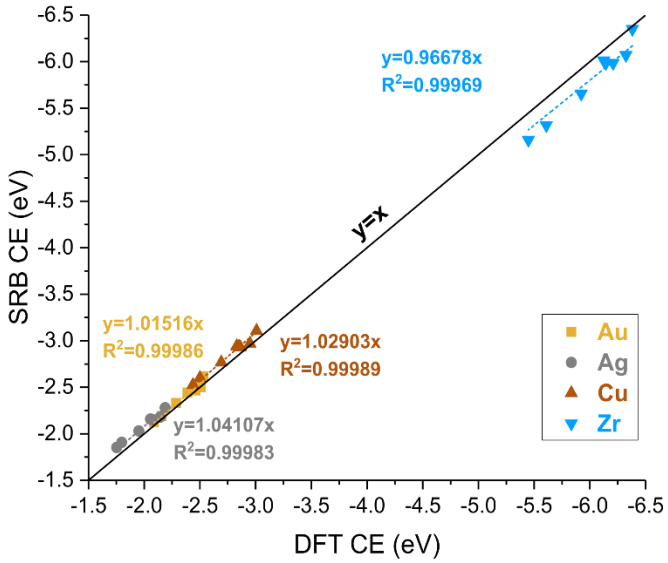

Figure 3. Parity between the cohesive energy (CE) of the SRB model vs. DFT on Cu (brown triangles), Ag (gray circles), Au (gold squares) and Zr (blue triangles) MNPs shown in Figure 1.

Beyond these combined size/shape/metal comparison tests, we assessed the power of the SRB model to capture shape differences. In Figure 4, we compare the SRB model against DFT on 4 MNP structures of each metal with fixed size of 55 atoms but different shapes: Icosahedron (Ih), Decahedron (Dc), Pyramid (Py) and truncated Octahedron (Oh). A clear CE trend is observed for all metals: Ih < Dc < Oh < Py. This trend agrees perfectly with previous experimental and computational findings related to structure of MNPs at 55-atom size.[58-59] SRB model captures shape differences by differences in CNs of atoms in the MNP. Since smaller MNPs have higher percentage of undercoordinated atoms (See Appendix C Figure S1), shape differences have a higher impact on these MNPs. At 55 atoms we are testing a size where shape differences play a significant role.

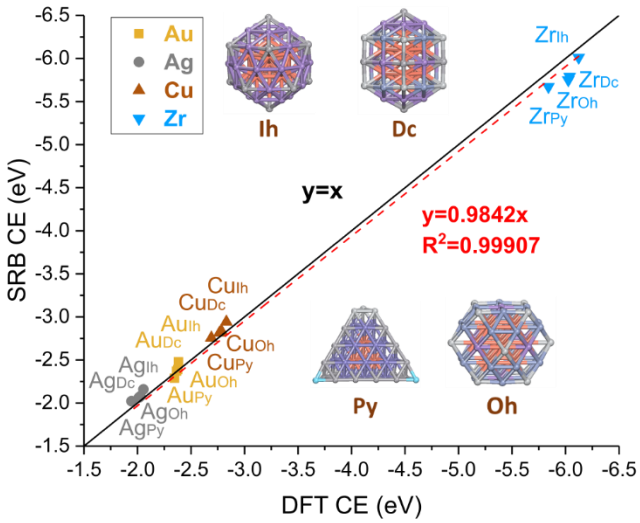

Figure 4. Parity plot between CE of the SRB model and DFT calculations of CE of MNPs of different shapes. All MNPs consist of 55 atoms and the different shapes are illustrated as insets in the plot (Ih=Icosahedron, Dc=Decahedron, Py=Pyramid, Oh=Octahedron).

With the SRB model effectively modeling both MNP shape and size effects, we see the SRB as an effective theory in rationalizing MNP morphology and of interest in a variety of MNP applications.[15, 60]

3.3 NANOALLOYS

Moving past monometallic MNPs, we turn our focus to Nanoalloys whose morphology, composition and chemical ordering represent key variables for many applications.[21-22] To rationalize nanoalloy behavior, we move beyond atom-centric SRB model and utilize our new BC model. We tested the performance of the BC model in comparison to SRB model against DFT calculations over a series of CuAg and CuZr nanoalloy MNPs of varying size, shape and

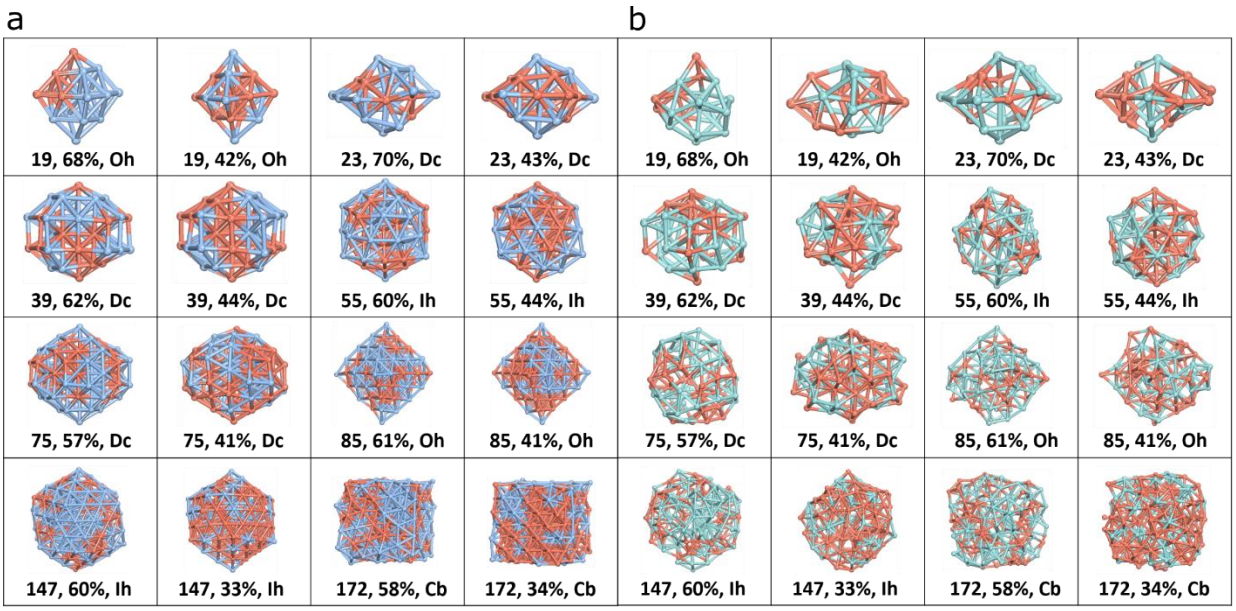

Figure 5. (a) CuAg and (b) CuZr nanoalloys of different size, shape, and composition. Structures depicted have been relaxed with DFT calculations. Red represents Cu, blue represents Ag and green represents Zr. The label indicates MNP size (total number of atoms), and percentage of Ag/Zr in the nanoalloys (Oh=Octahedron, Dc=Decahedron, Ih=Icosahedron, Cb=Cubic).

composition as shown in Figure 5. The composition and chemical ordering of the structures in Figure 5 were randomly assigned resulting a wide range of ordering and compositions. From Figure 5, we note that the CuZr structures became more distorted (amorphous) after DFT relaxation than the equivalent CuAg structures. This is because Cu and Zr have larger difference in atomic radius than Cu and Ag. To capture this restructuring accurately with CNs, we created a general CN determination code as described in the section 3.1. This code is able to capture the atomic radius effect and assign CN to arbitrary nanoalloy structures. Figure 6 shows the CE result predicted by BC and SRB models against DFT calculations over nanoalloy structures presented in Figure 5. From Figure 6, we note the BC model captures the DFT energetics more accurately than the SRB model for both nanoalloy systems. We calculated the average difference between the models as:

$$Avg_{diff} = \frac{\sum_1^N |CE_i^{BC} - CE_i^{SRB}|}{N} \quad (3\text{-}1)$$

where N is the number of nanoalloy structures tested. The average difference between the two models is 0.07 eV/atom in the CuAg case and 0.098 eV/atom in the CuZr case. This indicates a 1.3-1.9 eV improvement in total nanoalloy energetics for the smallest system (19 atoms) and a substantial 12-17 eV improvement for the largest system (172 atoms). The difference between the

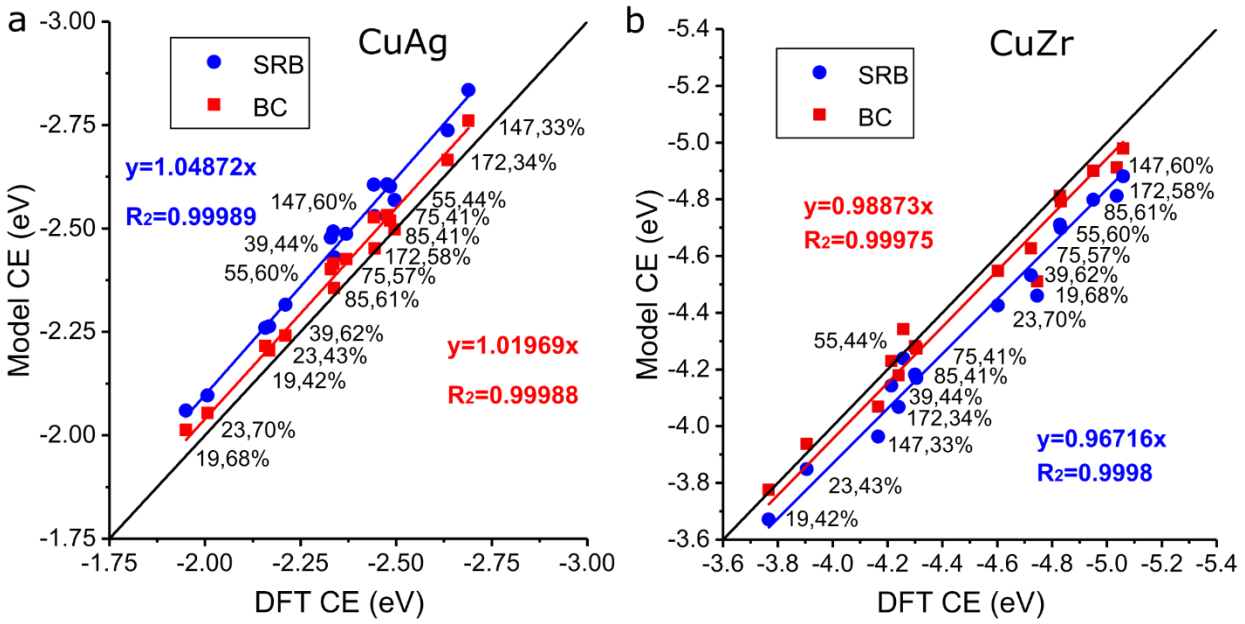

Figure 6. Parity plot between both the BC and SRB models with DFT CEs on (a) CuAg and (b) CuZr alloy MNPs. Labels indicate MNP size (total number of atoms) and %Ag in the CuAg nanoalloys, and %Zr in the CuZr nanoalloys.

models is directly related to the percentage of heterolytic bonds in the alloy as the BC model is mathematically identical to the SRB model for hemolytic bonds. We highlight an extreme demonstration of the effect of chemical ordering on the accuracy of the BC vs SRB models in Figure 7 where we compare two nanoalloys with identical size (172), similar shape (Cubic), and

similar composition (~50% Cu/Zr). The nanoalloy that has relatively few heterolytic bonds (Janus-type) shows little difference (~0.02 eV) between the SRB and BC models, while the nanoalloy with many heterolytic bonds (interlayer-mixed MNP) shows a substantially (5X) larger difference (~0.1 eV). Weighting hetetolytic bonds in the BC model therefore increases its ability (relative to SRB) to accurately describe chemical ordering effects. The advantage of BC model in capturing chemical ordering effect is further illustrated in section 3.3 on FePt nanoalloys.

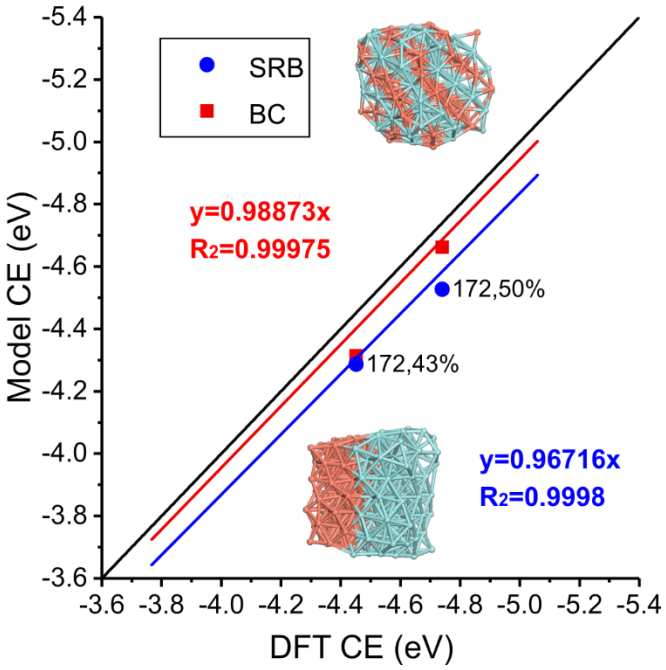

Figure 7. Chemical ordering comparison between two CuZr alloy MNPs. The MNP at the bottom is "Janus-type" while the MNP at the top is "interlayer-mixed". The size (172) and %Zr of the MNPs are given as data labels. The equations of fit shown are identical to those on Figure 6b and are included for reference.

In addition to CE, we further tested the BC model in describing mixing energetics of metals via EE analysis. EE in equation (2-1) describes the tendency to form a mixed alloy than 2 separate monometallic particles. Figure 8 shows the EE values predicted by BC model against DFT

calculations over all the CuAg and CuZr structures presented in Figure 5. In Figure 8, we see that the BC model captures the EE in good agreement with accurate DFT calculations with R^2 value close to 0.7 which is typical threshold for statistical significance). The two points far above the parity line in the second quadrant of Figure 6 are both $Cu_{147-x}Zr_x$ nanoalloys and these points are predicted higher in EE by the BC model largely due to the relative overestimation of the Zr_{147} MNP CE by the SRB model (most upper-right point on Figure 3). Therefore, the deviation observed in Cu_xZr_y excess energies is likely more strongly related to individual MNP structure than to model parameters. If these two points are removed, the R^2 of the equation of fit becomes greater than 0.8, highlighting the remarkable accuracy of the BC model for capturing mixing in even amorphous structures.[52] Therefore, the BC simply, computationally fast, and (relatively) accurately captures nanoalloy EE.

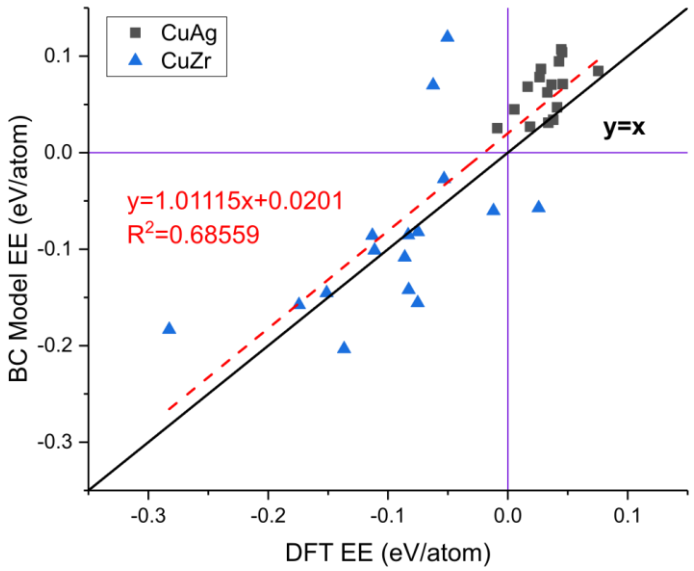

Figure 8. Parity between excess energy (EE) calculated by the BC model vs. DFT of CuAg (black squares) and CuZr (blue triangles) nanoalloy (shown in Figure 4).

3.4 BEYOND REACH OF DFT

Due to the speed and ease of applying BC model, we move on to utilize BC model to study energetics of a nanoalloy whose size is beyond the reach of DFT. The FePt nanoalloy is an experimentally-determined structure containing 23196 atoms in total (6569 Fe atoms and 16627 Pt atoms) and was published by Y.Yang et.al.[21] This nanoalloy is computationally inaccessible by current DFT methods due to its size and almost countless number of homotops. Using the BC model, though, we can rapidly screen and analyze the energetics of this enormous FePt nanoalloy. To generate testing structures, we used our CN-determining code to create a binding topology for the experimental nanoalloy structure and a homotop-generator using Python script able to randomly (or conditionally) distribute atoms inside the nanoalloys and calculate the resulting CE and EE. Note that we generated about 23,000 homotops as presented in Figure 9 and the BC model completed all energetic calculations within minutes. Figure 9a shows the EEs of both the experimental FePt nanoalloy structure and 3 sets of generated homotops vs. %Fe using our BC model. The black squares represent the lowest-energy structures of all tested alloy MNPs for a given %Fe, which happen to all have the Fe atoms distributed to the lowest coordination sites. The red dots show the minimum-energy structures of fully-randomized homotops and the blue triangles the energy of the structures with the experimental percentage of the total Fe atoms (2685/6569≈40.8%) distributed on the nanoalloy surface and randomized bulk atomic positions. Except for the experimental nanoalloy, every point presented in Figure 9a represents the minimum energy of one thousand structures generated using the same criteria. In all generated nanoalloys cases the EE is roughly parabolic with the Fe concentration, giving minima around 50% for the fully-random case and around 55% for the other two cases. This parabolic shape and minima around 50% Fe exactly match a recent DFT study of EE in smaller 55-atom FePt nanoalloys.[61]

Moreover, the EE is negative over the full composition range indicating favorability of forming intermixed nanoalloys instead of having separate monometallic MNPs, which matches perfectly with experimental observations.[21] In addition, if we look at vertical slice of the Figure 9a plot (i.e. a fixed percentage of Fe), EE becomes more negative as the %Fe distributed on the surface increases, indicating Fe is generally more favored towards surface segregation. The effects of surface segregation and chemical ordering are presented more clearly in Figure 9b and 9c.

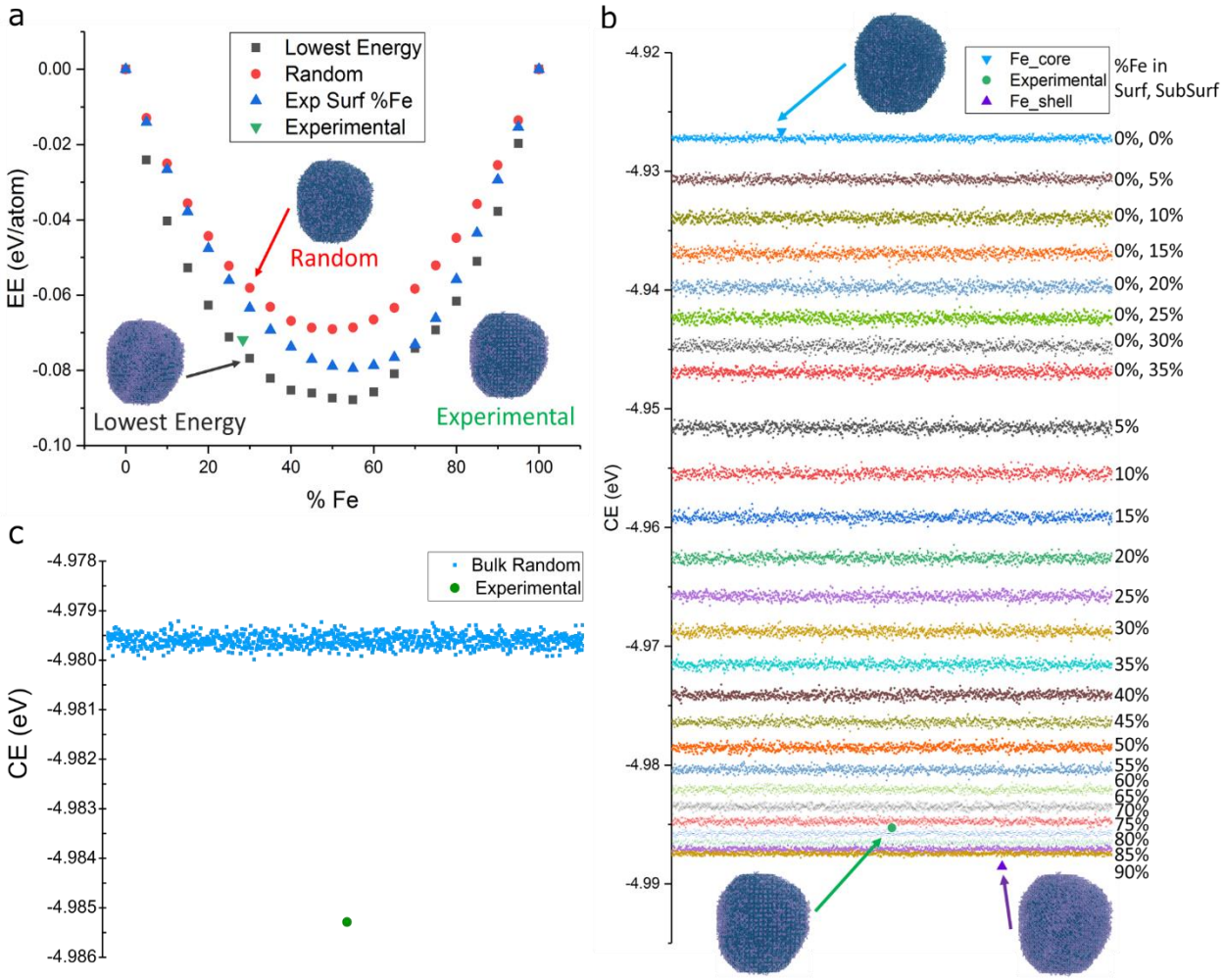

Figure 9. (a) Excess Energy (EE) (eV/atom) versus % Fe composition in the FePt alloy MNP. The black points represent the lowest-energy structures tested at each composition, which were all structures with Fe atoms placed in the lowest coordinated sites. The red points represent the minimum energy structure of 1,000 fully random homotop structures. The blue points represent the minimum energy structure of 1,000 randomly generated structures with same % surface Fe as the experimental structure (randomly distributed in the surface) with the rest of Fe atoms equally and randomly distributed into the subsurface and bulk of the MNPs. The images shown as insets are examples at the experimental composition of the random, lowest energy, and experimental structures where Fe is dark blue and Pt is purple. (b) CEs of randomly created homotops of the experimental FePt nanoalloy.[3] The purple triangle represents an Fe-shell structures (i.e. black point in (a)) while the light blue triangle represents an Fe core structure, where all Fe atoms are in the bulk of the MNP. Each band represents 1000 randomly created structures with specific percentages of surface/subsurface/bulk atoms occupied by Fe atoms. All structures contain same ratio of Pt to Fe. (c) CE (eV) of randomly generated FePt alloys (blue points) with an identical surface/subsurface to the experimental structure with Fe randomly distributed in the bulk atoms. The images shown as insets show the representative nanoalloy structures with Fe as dark blue and Pt as purple. The green point represents the experimental structure in (a-c).

Figure 9b shows a systematic analysis of surface segregation through a "rainbow" plot of how CE changes with the distribution of Fe into different layers (surface, subsurface, and bulk). Starting from the surface (CN≤9), the Fe atoms are gradually distributed into subsurface (CN=10,11) and finally distributed into the bulk (CN=12). It is clearly shown in Figure 9b that CE gets more negative as more Fe atoms are distributed into lower-coordinated sites (same as the EE trend). This is because both BC and SRB model predict atoms with more negative CE_{bulk} value (Pt in this case) tend to stay in the bulk and atoms with less-negative CE_{bulk} values tend to be surface segregated. However, the CE_{bulk}value is not the only factor affecting energetics of nanoalloy structures. The difference between bands represent the energetic effects of Fe segregation caused by bulk CE value but the deviation within each band is caused by chemical ordering effects. Beyond this argument, we note that the experimental structure (green points in Figure 9), which is 28.3% Fe with only 43.4% of Fe atoms in the surface, has significantly higher CE than its corresponding band (homotops with same %Fe in the surface). Surprisingly, the experimental structure is close to the minimum-energy structure we created with all Fe atoms distributed into the lowest coordinated sites. This indicates chemical ordering effect is another significant factor in addition to bulk CE values in this FePt nanoalloy and that the structure with experimental chemical ordering is preferentially formed during the experiment. Figure 9c is a clearer example of the significance of chemical ordering and the ability of the BC model to capture it. Figure 9c shows the CEs of the experimental structure of 1000 homotops with an identical surface conformation (atoms at identical position as experimental structure in both surface and subsurface layer). All structures in Figure 9c have the same CNs, surface, and subsurface structures, so the only variable between each point is the chemical ordering of the bulk atoms. We can see that the BC model captures the deviation of homotops within the band, whereas by design, the SRB model

gives identical values for structures with same coordination environment. In addition, we can see the distinctiveness of the experimental conformation, as it is several standard deviations from these randomized homotops, indicating chemical ordering in the bulk plays a vital role in forming the experimentally-observed FePt alloy.

In conclusion, the BC model is able to capture the surface segregation effect though Bulk CE values and chemical ordering effect through difference in bonds on the experimental FePt nanoalloy and its homotops whose size and quantity are beyond the reach of DFT.

3.5 APPLICABILITY AND LIMITATIONS

In the above sections, we proved our BC model a promising model for CE and EE prediction in a wide range of nanoalloys. However, like every other model, our BC model has its own applicability and limitations. In this section, we discuss the BC model's applicability and limitations either from assumptions we made in the design of the model or from DFT calculated CE_{Bulk} values. We also discuss ways to overcome some of the limitations.

First, when designing bond weight factors (γs) in the BC model, we assume homolytic dimer BDE trends match the CE_{bulk} trends for metals. This means that when the dimer BDEs of elements in a heterolytic bond trend opposite to their corresponding CE_{bulk} values, the bond weight factors will give incorrect CE trends for homolytic vs. heterolytic bond energies. To qualitatively show the applicability of our BC model, we plot homolytic dimer BDEs vs. CE_{bulk} values for all transition metals in Figure 10. Note that all values in Figure 10 are experimental values. Pairs of elements with positive slopes in Figure 10 are good candidates for the BC model, while pairs of elements with negative slopes are not. After applying this criterion to pairs of metals plotted in

Figure 10, we found 55 “bad candidate” bimetallic alloys versus a remarkable 296 that are well-suited for the BC model, meaning around 85% of transition metal alloys are hypothetically captured by the BC model. This analysis reveals that nanoalloys that exclusively contain a subset of elements Au, Ag, Cu, Zr should all be accurately captured by the BC model, while a nanoalloy containing only Cu and Pd would not. For “bad candidate” nanoalloys, we suggest applying SRB model by setting γs to 1. It will give roughly accurate predictions but cannot capture bulk chemical ordering effect as presented in Figure 9c.

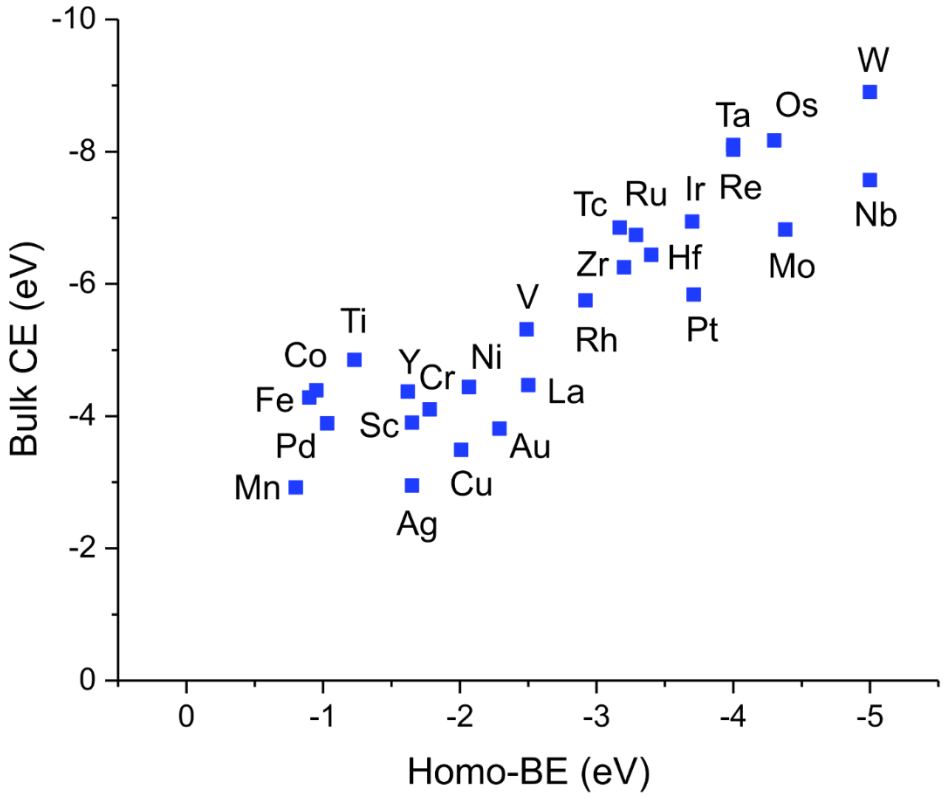

Figure 10. Bulk Cohesive Energy (CE_{Bulk})[1] versus Homolytic dimer bond dissociation energy (BDE)[2] of various transition metals.

We have also identified cases where limitations in DFT (PBE functional) resulted in deviations in comparative BC predictions. For example, in Figure 11a and S2a (Appendix C), the BC model appears to fail to predict DFT CE of CuAu alloys. In this case, in terms of experimental BDE, we have AuCu > AuAu > CuCu and the calculated weighting factors (eqs. 2-5 and 2-6) are γ_{Au}=2.36 and $\gamma_{Cu} = -0.36$. However, the CE_{bulk} trend between Au and Cu according to DFT is opposite to the experimental CE_{bulk} trend, largely due to the DFT underestimation of the Au bulk CE (Figure 2b). Thus, the BC model appears to behave weaker than the simple SRB when compared to DFT, though we would like to highlight that this deviation reflects error in the DFT functional performance rather than the BC model. Beyond AuCu, another case where the underestimation of the CE_{bulk} of Au by DFT shifts the BC model away from parity with DFT is for AuAg nanoalloys (see Figures 11b and S2b in Appendix C). In the AuAg nanoalloy we highlight both the BC and SRB models do remarkably well in capturing DFT energetics, though the SRB appears to be a slightly better match with DFT than the BC. Under the same assumption of the CE_{bulk} values trending with the dimer BEs used in the BC model, an underestimated CE_{bulk} for Au relative to Ag would result in a slight overestimation of the CEs of AuAg alloys MNPs.

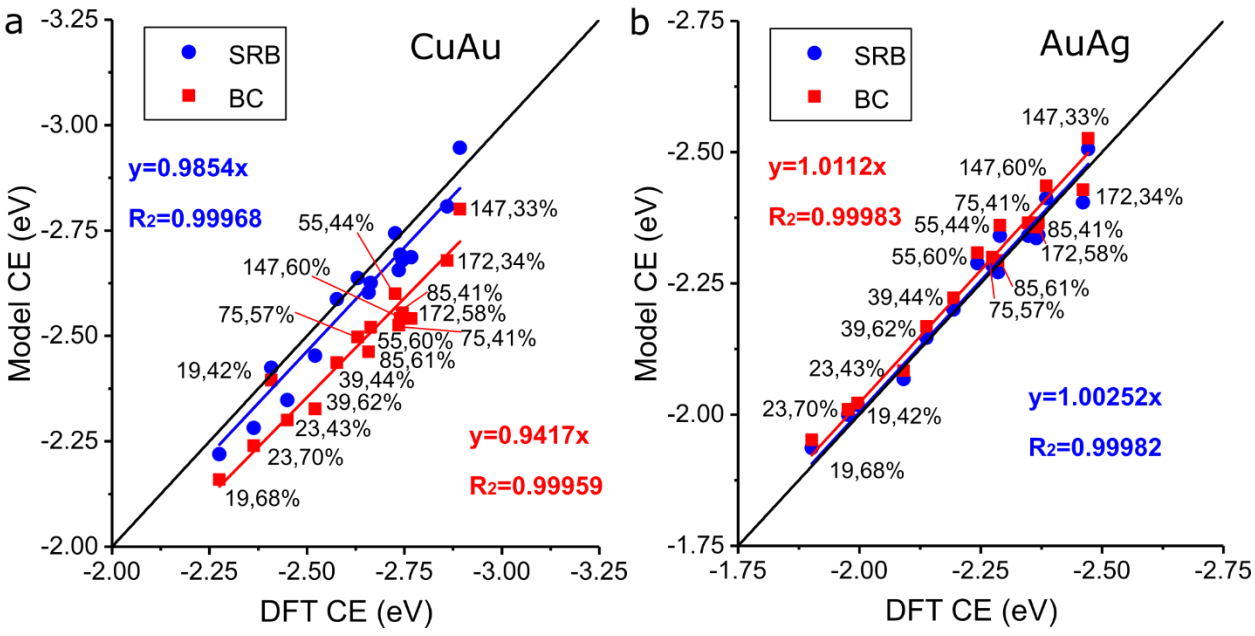

Figure 11. Parity plot between both the BC and SRB models with DFT CEs on (a) CuAu and (b) AuAg alloy MNPs. Labels indicate MNP size (total number of atoms) and %Au in the CuAu nanoalloys, and %Ag in the AuAg nanoalloys.

While we believe our selection of DFT functional for this work is appropriate, the use of other, potentially more accurate functionals like revPBE and PBEsol, could increase the accuracy of the SRB and BC models for capturing nanoparticle energetics vs. DFT. Additionally, such an adaptation to the SRB/BC models would require only the new CE_{bulk} values for the metals of interest calculated at the new level of theory. Eventually, when compared with experimental energetic data, experimental CE_{bulk} values will be applied instead of DFT values. To further validate the BC model against experimental behavior for the CuAu MNPs we tested the surface segregation behavior in CuAu MNPs (Figure 12a). Here we use surface segregation energy (SE) as an energetic factor to describe surface segregation behavior. SE is the energy required to move an atom from surface to bulk and more negative SE indicates higher tendency of an atom to stay on surface. In the $Cu_{54}Au$ MNP (Figure 12b), the Au is shown to have a favorable surface

segregation in experiments[62] by both DFT and the BC model (using experimental values of CE_{bulk}), and unfavorable surface segregation by the SRB model (using experimental values of CE_{bulk}). Since the SRB model only accounts for coordination number and not chemical environment, it favors Au to be in bulk because the experimental CE_{bulk} of Au is larger than the CE_{bulk} of Cu (Figure 2b). We note that DFT predicts a favorable Au surface segregation mainly because the DFT-calculated CE_{bulk} for Au is incorrectly less than for Cu (Figure 2b), indicating that in an alloy, Au would naturally surface segregate (according to simple surface energy arguments). Therefore, the BC model alone accurately captures experimental segregation in AuCu alloy MNPs, clearly for physical reasons.

a

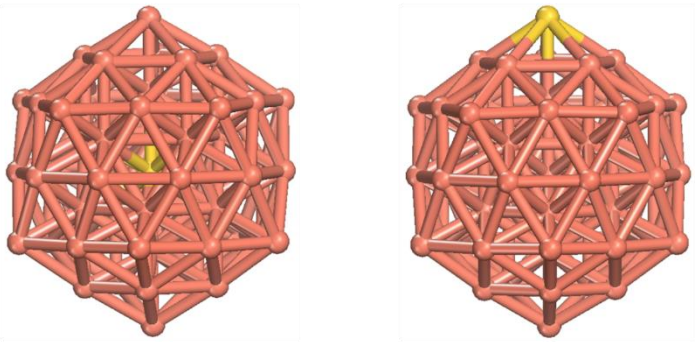

$Cu_{54}Au_C$ $Cu_{54}Au_T$

b

	CE $Cu_{54}Au_C$	CE $Cu_{54}Au_T$	SE
DFT	-2.800 eV	-2.831 eV	-1.686 eV
BC model	-2.932 eV	-2.937 eV	-0.316 eV
SRB model	-2.923 eV	-2.922 eV	0.0937 eV

Figure 12. (a) DFT-optimized geometries of Cu54AuC (Au – Center) and Cu54AuT (Au -Top) (b) Table of CEs and surface segregation energetic behavior (SE) in CuAu MNPs with BC, SRB, and DFT models.

To summarize, we addressed the applicability and limitations of our BC model in this section. We highlight that the limitations of DFT do not influence the BC model predictions when the latter is applied using only experimental CE_{bulk}values. In addition, energy stability trends between different MNPs are most often more important than exact precision in energetic stability and the BC model accurately captures trends in alloy MNPs.

4.0 CONCLUSIONS

In this thesis, a new thermodynamic (Bond-Centric, BC) model is introduced able to accurately capture the energetics of MNPs, as well as their mixing behavior. We performed comprehensive tests on the BC model over a wide series of nanoalloys against an existing SRB model and DFT. The BC model is orders of magnitude faster than DFT and significantly more accurate than SRB model in evaluating alloy MNPs of nearly any morphology (size, shape) and metal composition. Importantly, the BC model can identify energetically-preferred chemical ordering in alloy MNPs. To demonstrate the power of the BC model we performed CE and EE analysis over an experimental FePt nanoalloy and its homotops whose sizes and quantities are inaccessible by DFT. The results are in good agreement with literature. Additionally, because the BC model does not require training to calculated or experimental parameters it is uniquely suited to address the energetics in massive nanoalloy structures.

As CE is an enthalpy-driven energetic factor, our model doesn't account for entropy and temperature effects which are also important factors affecting surface segregation and chemical ordering behavior in nanoalloys. In the future, we will include entropy and temperature factors to the BC framework to make our model more tunable for broader applications. In conclusion, our work introduces a simple, yet very powerful tool for nanoalloy design that can potentially help elucidating the energetics of alloy MNP genome.

APPENDIX A

EXAMPLE OF CP2K INPUT FILES

A.1 INP FILE (EXAMPLE Au_{19})

```
&FORCE_EVAL
 METHOD QS
 &DFT
  UKS .TRUE.
  BASIS_SET_FILE_NAME /opt/sam/cp2k/2.6/data/BASIS_MOLOPT
  POTENTIAL_FILE_NAME /opt/sam/cp2k/2.6/data/GTH_POTENTIALS
  &MGRID
   CUTOFF 500
   REL_CUTOFF 60
   NGRIDS 4
  &END MGRID
  &QS
   EPS_DEFAULT 1.0E-14
   MAP_CONSISTENT
  &END QS
 &SCF
  SCF_GUESS ATOMIC
```

```
  EPS_SCF 1.0E-6
  MAX_SCF 500
  ADDED_MOS  200
  CHOLESKY INVERSE
  &SMEAR  ON
     METHOD FERMI_DIRAC
     ELECTRONIC_TEMPERATURE [K] 700
  &END SMEAR
  &DIAGONALIZATION
      ALGORITHM STANDARD
  &END DIAGONALIZATION
  &MIXING
      METHOD BROYDEN_MIXING
      ALPHA   0.1
      BETA    1.5
      NBROYDEN  8
  &END MIXING
&END SCF
```

```
  &XC
    &XC_FUNCTIONAL PBE
    &END XC_FUNCTIONAL
  &END XC
  &POISSON
    POISSON_SOLVER WAVELET
    PERIODIC NONE
  &END POISSON
&END DFT
&SUBSYS
  &CELL
    ABC  40.00000  40.00000  40.00000
    ALPHA_BETA_GAMMA    90.00    90.00    90.00
    PERIODIC NONE
  &END CELL
  &TOPOLOGY
    COORD_FILE_NAME zihao.xyz
    COORDINATE XYZ
```

```
    &END TOPOLOGY
    &KIND Au
      ELEMENT   Au
      BASIS_SET DZVP-MOLOPT-SR-GTH-q11
      POTENTIAL GTH-PBE-q11
    &END KIND
  &END SUBSYS
&END FORCE_EVAL
&GLOBAL
  PROJECT zihao
  RUN_TYPE GEO_OPT
  PRINT_LEVEL MEDIUM
&END GLOBAL
&MOTION
  &GEO_OPT
    MAX_FORCE 0.0004
    MAX_ITER 500
    OPTIMIZER BFGS
```

```
  TYPE MINIMIZATION

 &END GEO_OPT

&END MOTION
```

A.2 XYZ FILE (EXAMPLE Au_{19})

19

Au	17.960000000000001	17.960000000000001	20.000000000000000
Au	17.960000000000001	20.000000000000000	17.960000000000001
Au	15.920000000000002	20.000000000000000	20.000000000000000
Au	17.960000000000001	20.000000000000000	22.040000000000003
Au	17.960000000000001	22.040000000000003	20.000000000000000
Au	20.000000000000000	17.960000000000001	17.960000000000001
Au	20.000000000000000	15.920000000000002	20.000000000000000
Au	20.000000000000000	17.960000000000001	22.040000000000003
Au	22.040000000000003	17.960000000000001	20.000000000000000
Au	20.000000000000000	20.000000000000000	15.920000000000002
Au	20.000000000000000	22.040000000000003	17.960000000000001
Au	22.040000000000003	20.000000000000000	17.960000000000001
Au	20.000000000000000	20.000000000000000	20.000000000000000
Au	20.000000000000000	22.040000000000003	22.040000000000003
Au	22.040000000000003	20.000000000000000	22.040000000000003
Au	22.040000000000003	22.040000000000003	20.000000000000000
Au	20.000000000000000	20.000000000000000	24.080000000000002
Au	20.000000000000000	24.080000000000002	20.000000000000000
Au	24.080000000000002	20.000000000000000	20.000000000000000

APPENDIX B

DERIVATION OF EXCESS ENERGY (EE) AS A FUNCTION OF CE

For bimetallic alloy MNP, A_xB_y, the definition of cohesive energy (CE) is:

$$CE_{alloyMNP} = \frac{E_{alloyMNP} - xE_A - yE_B}{x+y} \quad (1)$$

Where E_X represents an energy of species X, x represents the number of atoms of type A and b represents the number of atoms of type B. Multiplying both sides of SI eq 1 by (x+y) we have:

$$E_{alloyMNP} = (x+y)CE_{alloyMNP} + xE_A + yE_B \quad (2)$$

On the other hand, the excess energy (EE) is expressed as:

$$EE = \frac{E_{alloyMNP} - \frac{x}{x+y}E_{A_{x+y}} - \frac{y}{x+y}E_{B_{x+y}}}{x+y} = \frac{E_{alloyMNP} - A\%E_{A_{x+y}} - B\%E_{B_{x+y}}}{x+y} \quad (3)$$

Where A_{x+y} is a monometallic A MNP and B_{x+y} , a monometallic B MNP.

Substituting the definition of $E_{alloyMNP}$ (SI eq 2) for each of the monometallic and alloy MNPs in SI eq 3 gives:

$$EE = \frac{(x+y)*CE_{alloyMNP} + xE_A + yE_B}{x+y} - \frac{x*[(x+y)(CE_{A_{x+y}}) + (x+y)(E_A)]}{(x+y)(x+y)} - \frac{y*[(x+y)(CE_{B_{x+y}}) + (x+y)(E_B)]}{(x+y)(x+y)} \quad (4)$$

and finally after further simplifying SI eq 4 we are left with:

$$EE = CE_{alloyMNP} - \frac{x}{x+y} CE_{A_{x+y}} - \frac{y}{x+y} CE_{B_{x+y}} \quad (5)$$

which is the definition of EE per atom used in the manuscript.

APPENDIX C

SUPPORTING FIGURES

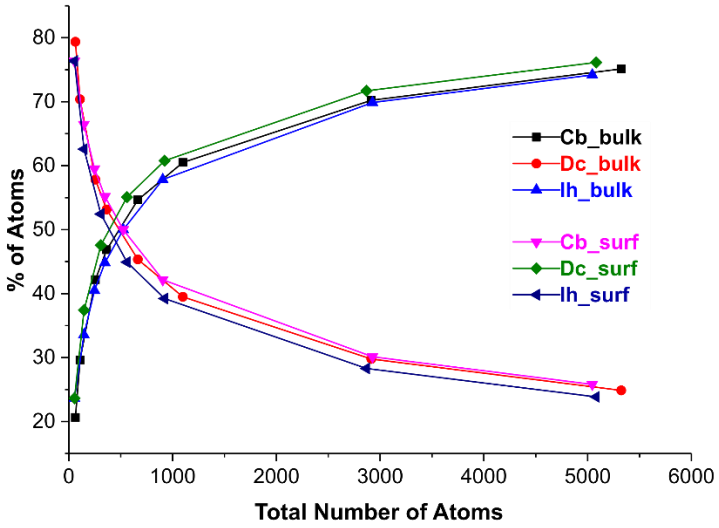

Figure S1. Percentages of bulk and surface atoms for MNPs with various sizes and morphologies.

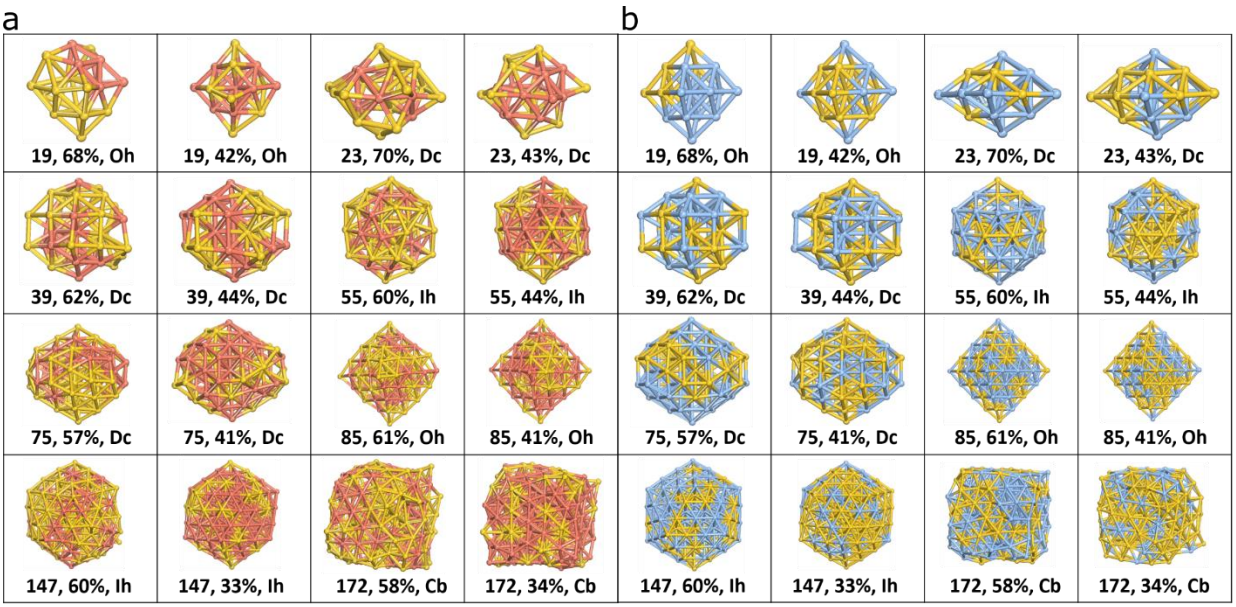

Figure S2. (a) CuAu and (b) AuAg alloy MNPs of different size, shape and composition. Red represents Cu, blue represents Ag and gold represents Au. The label indicates MNP size (total number of atoms), and percentage of (a) Au and (b) Ag atoms in the MNPs (Oh=Octahedron, Dc=Decahedron, Ih=Icosahedron, Cb=Cubic)

APPENDIX D

CODES

D 1 CN DETERMINATION CODE

```
#! /usr/bin/env python

# Tool for finding coordination numbers (cns) of metal nanoparticles (mnps) with arbitrary shapes

import ase

from ase.io import read,write

from ase.data import vdw_radii,chemical_symbols

from ase.atoms import *

from ase.calculators.neighborlist import *

import numpy as np

import sys


# Input: .xyz file of mnp (call this script with a .xyz file as the first argument)

# Output: modified .xyz file with average cn and radii scales along in the header 2 extra columns

# extra column 1 = cn value for every atom, extra column(s) 2 = neighbor list of every atom
```

```
# Notes:
# This code assigns a bimetallic mnp as amorphous if the ratio of vdw_radii of 2 elements is < 1.1.
#######################################
# For amorphous structures, the code will keep decreasing atomic scales until 1 atom has cn>12, except
# when no smaller atoms are in the bulk (i.e. a Zr-core structure for a CuZr MNP)
# the maxinum number of atoms with cn>12 allowed to be num_total_atoms^(1/3).
# The upper limit for  maximum cn is 13.
# In general, scales of the atoms with more cn>12 deviations are preferentially reduced, except
# for structures with all larger atoms on surface/subsurface, the larger atom will take priority in cutting.
#####################################################################
# if a mnp is not amorphous the code will keep decreasing the scale until no atom will have cn>12
#####################################################################
# for pure metals, the start scale is 0.875 instead of 1 to get more accurate cn results.
# so the scale starting at 0.875 works for all elements and structures tested thusfar.
#####################################################################
# Vdw_radii for metals taken from:
# Hu, S. Z.; Zhou, Z. H.; Robertson, B. E., Consistent approaches to van der Waals radii for the
# metallic elements. Zeitschrift Fur Kristallographie 2009, 224 (8), 375-383.
#####################################################################
```

```
if len(sys.argv) <1:
    print 'Error: Not enough arguments passed!'
    sys.exit()


count_0=0
newvdw=[ 0. , 0. , 0. , 2.14, 1.69, 1.68, 0. , 0. , 0. ,
       0. , 0. , 2.38, 2. , 1.92, 1.93, 0. , 0. , 0. ,
       0. , 2.52, 2.27, 2.15, 2.11, 2.07, 2.06, 2.05, 2.04,
       2. , 1.97, 1.96, 2.01, 2.03, 2.05, 2.08, 0. , 0. ,
       0. , 2.61, 2.42, 2.32, 2.23, 2.18, 2.17, 2.16, 2.13,
       2.1 , 2.1 , 2.11, 2.18, 2.21, 2.23, 2.24, 0. , 0. ,
       0. , 2.75, 2.59, 2.43, 0. , 0. , 0. , 0. , 0. ,
       0. , 0. , 0. , 0. , 0. , 0. , 0. , 0. , 0. ,
       2.23, 2.22, 2.18, 2.16, 2.16, 2.13, 2.13, 2.14, 2.23,
       2.27, 2.37, 2.38, 2.49, 0. , 0. , 0. , 0. , 0. ,
       2.45, 0. , 2.41, 0. , 0. , 0. , 0. , 0. , 0. , 0. ]


# Step_size parameter determines how much the radii will be shifted when CN exceptions occur
step_size=-0.001
# Difference between changes in scales for more frequent element that has higher cn than 12
difference=0.3
```

```
def cns(neiglist):
    cns=[]
      complete_nl=[] #include neighborlist of all atoms
    for i in range(len(atoms1)):
            neighs=neiglist.get_neighbors(i)
            neighs=neighs[0].tolist()
            neighs=[x for x in neighs if x != i]
            #print neighs
            cns.append(len(neighs))
            complete_nl.append(neighs)
            #print final_nl
      return np.array(cns), np.array(complete_nl) #turn into an array


for item in range(1,len(sys.argv)):
    # Set a scaling so that the cns code will automatically adjust
    # outflag used to determine if a scale has been set for both elements that makes all cns < 12
    outflag=0
      nl=None
      moleculename=sys.argv[item]
      atoms1=read(moleculename)
      atomic_numbers=atoms1.get_atomic_numbers()
      num_atoms=len(atomic_numbers)
      max_more_num=int(num_atoms**(1./3)) #max num of atoms allowed with CN>12
```

```
# min and max anums determine the identify of the bimetallics
min_anum=min(atomic_numbers)
max_anum=max(atomic_numbers)
    # The following line are calculating ratio of vdw_radii of elements
    vdw_radi_1=newvdw[min_anum]
    vdw_radi_2=newvdw[max_anum]
# Decide "larger" atom by comparison of vdw_radii of elements
    if vdw_radi_1>vdw_radi_2:
            large_atom=min_anum
            small_atom=max_anum
    else:
            large_atom=max_anum
            small_atom=min_anum
    min_vdw_radi=min(vdw_radi_1,vdw_radi_2)
    max_vdw_radi=max(vdw_radi_1,vdw_radi_2)
    ratio_vdw_r=max_vdw_radi/min_vdw_radi
# Determine if pure metal MNP - set initial scales to 0.875
# scale_1 assigned to the smaller element in bimetallic MNP
# scale_2 assigned to the larger element in bimetallic MNP
    if ratio_vdw_r==1:
            scale_1=0.875
            scale_2=0.875
    else:
```

```
            scale_1=1
            scale_2=1
####### New Section ###################
while outflag==0: # While used to continue loop until outflag is true
    cutoffs=[]
  # Generate cutoffs by atomic_numbers
    for i in range(len(atomic_numbers)):
    temp=atomic_numbers[i]
    if temp==min_anum:
        cutoffs.append(scale_1*newvdw[temp])
    else:
            cutoffs.append(scale_2*newvdw[temp])
  # update neighborlist and calculate new cns
    nl=NeighborList(cutoffs,bothways=True,skin=0.0)
    nl.update(atoms1)
    cordns,final_nl=cns(nl) #final_nl = complete_nl
  # countmin/max are counters for the number of atoms which have cns>12
  count_small=0
  count_large=0
  less=0
    more=0
    too_much=0 #atom with CN>13
    bulk_large=0
```

```
    bulk_small=0
for i in range(len(cordns)):
    # Check if the cn of atom i is greater than 12 or less than 3
        if cordns[i]<3:
            less+=1
        if cordns[i]>13:
            too_much+=1
    if cordns[i]>12:
        # Check element of atom i that has deviated from normal CN range
        more+=1
        if atomic_numbers[i]==small_atom:
            count_small+=1
        else: count_large+=1
            if cordns[i]>=12 and atomic_numbers[i]==large_atom:
                bulk_large+=1 #looking for large atoms in the bulk
            if cordns[i]>=12 and atomic_numbers[i]==small_atom:
                bulk_small+=1
# check if any of the counters were incremented (i.e. if any atoms were CN>12 or CN<3)
    if ratio_vdw_r >=1.1: #when ratio>=1.1, the structure is "amporphous":
        if bulk_small==0:#when all small atoms are not in bulk
                if (count_large+count_small)>max_more_num or too_much>0:
                    scale_2+=step_size
                    scale_1+=step_size*difference
```

```
                else:
                        outflag=1
        elif bulk_large==0: # No large atoms in the bulk (all large atoms on surface)
                if (count_large+count_small)>0: # No overcutting will happen in this case,
to cut down to 0
                        scale_2+=step_size
                        scale_1+=step_size*difference
                else:
                        outflag=1
        elif (count_large+count_small)>max_more_num or too_much>0:
    # If any are, increment their scale by the the step_size, favor "larger" element
                if count_large>=count_small:
                        scale_2+=step_size
                        scale_1+=step_size*difference
                else:
                        scale_1+=step_size
                        scale_2+=step_size*difference
                else: outflag=1
    # set outflag=1 to exit while loop!
        elif ratio_vdw_r==1.0: # Only true if this is a pure metal MNP, reduce scale factor
                if (count_large+count_small)>0:
                        scale_2+=step_size
                        scale_1=scale_2
```

```
            else: outflag=1
        else: #Structure is not over distorted
            if (count_large+count_small)>0:
        # if any are, increment their scale by the the step_size, favor "larger" element
            if count_large>=count_small:
                    scale_2+=step_size
                    scale_1+=step_size*difference
            else:
                    scale_1+=step_size
                    scale_2+=step_size*difference
            else: outflag=1
################################################
# Read and write out the _cns.xyz file
    file1=open(moleculename,'r')
    lines=file1.readlines()
    file1.close()
    outname=moleculename.replace(".xyz","",1)
    file2=open('{} _cns.xyz'.format(outname),'w')
    count=0
    for line in lines:
            if count==0:
                    file2.write(line)
                    count+=1
```

```
            elif count==1:
                file2.write('Average CN={} , Scale {} = {} , Scale {} = {}
\n'.format(cordns.mean(),
chemical_symbols[small_atom],scale_1,chemical_symbols[large_atom],scale_2))
                count+=1
            else:
                vect=line.split()
                a=float(cordns[count-2])
                b=final_nl[count-2]
                vect.append('{}'.format(a))
                vect.append('{}\n'.format(b))
                out=' '.join(vect)
                file2.write(out)
                count+=1
        file2.close()
    # Write out the name, scales, and average coordination number!
        print '{}  Scale {} = {},  Scale {} ={}, Avg CN=
{}\n'.format(outname,chemical_symbols[small_atom],scale_1,chemical_symbols[large_atom],sc
ale_2,cordns.mean())
```

D 2 BC SRB MODEL CODE

```
#!/usr/bin/env python

# Code for calculating the cohesive energy (CE), using the BC/SRB models, of Arbitrary Metal Nanoparticles (MNP)

# For details surrounding the module see 10.1021/acs.nanolett.8b00670

import numpy as np

import sys

import csv

import ase

import math

from ase.io import read,write


# This code calculates the cohesive energy of MNPs of 28 transition metals


# Input: modified .xyz file generated from cns code (call this script with the modified .xyz file as an argument)

# Output: Prints the cohesive energy (CE) of the MNP (in eV)


# Two references are used for bond dissociation energies (BDE)

# Reference 1: Morse, M. D., Clusters of transition-metal atoms. Chem. Rev. 1986, 86 (6), 1049-1109.
```

```
# Reference 2: Miedema, A. R., Model predictions of the dissociation energies of homonuclear and heteronuclear diatomic molecules of two transition metals. Faraday Symposia of the Chemical Society 1980, 14 (0), 136-148.

# Reference 1 is prefered because it is experimental values while reference 2 has predictions

# When data is not availible from reference 1, it will be used from reference 2


# read csv file and returns data as a matrix of floats

def csv_read(filename):

        dataraw = np.array(list(csv.reader(open(filename, "rb"), delimiter=",")))

        data_raw1=np.delete(dataraw,0,0) #delete first row and column

        data_pure=np.delete(data_raw1,0,1).astype("float")

        return data_pure


# Read in reference 1 and 2 data

WF_1=csv_read("WF_refer_1.csv")

WF_2=csv_read("WF_refer_2.csv")


# Dictionary of metals, with numbers assigned in sequence of element number

t_metals={"Sc":0,"Ti":1,"V":2,"Cr":3,"Mn":4,"Fe":5,"Co":6,"Ni":7,"Cu":8,"Y":9,"Zr":10,"Nb":11, \

        "Mo":12,"Tc":13,"Ru":14,"Rh":15,"Pd":16,"Ag":17,"La":18,"Hf":19,"Ta":20,"W":21,"Re":22, \

        "Os":23,"Ir":24,"Pt":25,"Au":26,"Th":27}
```

```
# Dictionary of Bulk Cohesive Energies (BCE)

# Reference: Charles Kittel. Introduction to Solid State Physics, 8th edition. Hoboken, NJ: John Wiley & Sons, Inc, 2005.


BCE={"Sc":-3.90,"Ti":-4.85,"V":-5.31,"Cr":-4.10,"Mn":-2.92,"Fe":-4.28,"Co":-4.39,"Ni":-4.44, \
        "Cu":-3.49,"Y":-4.37,"Zr":-7.1914,"Nb":-7.57,"Mo":-6.82,"Tc":-6.85,"Ru":-6.74 ,"Rh":-5.75, \
        "Pd":-3.89,"Ag":-2.95,"La":-4.47,"Hf":-6.44,"Ta":-8.10,"W":-8.90,"Re":-8.03,"Os":-8.17, \
        "Ir":-6.94,"Pt":-5.84,"Au":-3.81,"Th":-6.20}


# Check if not enough arguments passed
if len(sys.argv)<1:
    print "Wrong number of arguments passed. For example:call with ./BE_All_exp *.xyz"
    sys.exit()


for item in range(1,len(sys.argv)):
        moleculename=sys.argv[item]
        original=read(moleculename)
        atomicsymbols=original.get_chemical_symbols()
        atom_types=list(set(atomicsymbols))
        file1=open(moleculename,'r')
    # For ease of processing neighbors load all the lines into memory
```

```
lines=file1.readlines()
file1.close()
count=0
BE=0
for line in lines:
        if count<=1:
                count+=1
        else:
                vals=line.split()
        # Isolate CN value of atom i from modified .xyz file
                CN_i=float(vals[4])
                name_i=vals[0]
                BCE_i=BCE[name_i]
                t_metal_i=t_metals[name_i] #Pull out transition metal reference number
                i=count-2
        # Isolate neighborlist for each atom from modified .xyz file
                vect=line.split("[")
        nl_i_raw=vect[1][0:-2]
        nl_i_raw_2=nl_i_raw.split(",")
        nl_i = [int(i) for i in nl_i_raw_2]
        # Iterate over all nieghbors of i to evaluate the BC model.
                for j in nl_i: #j is a neighbor of i
              k=j+2
```

```
line_j=lines[k]
vals_j=line_j.split()
CN_j=float(vals_j[4])
name_j=vals_j[0]
        BCE_j=BCE[name_j]
        t_metal_j=t_metals[name_j]
        t=WF_1[t_metal_i][t_metal_j]
        if t != 0: #reference 1 is in priority since it's experimental value
            AB=t
            AA=WF_1[t_metal_i][t_metal_i]
            BB=WF_1[t_metal_j][t_metal_j]
        else: #Switch to reference 2 if reference 1 doesn't have the data
            AB=WF_2[t_metal_i][t_metal_j]
            AA=WF_2[t_metal_i][t_metal_i]
            BB=WF_2[t_metal_j][t_metal_j]
        if AA==BB: #i and j are same metal, SRB model
            bl_i=1
            bl_j=1
        else: #i and j are different metals, BC model
    # Calculate the gamma, weight factors
            bl_i=2(AB-BB)/(AA-BB)
            bl_j=2-bl_i
# Apply the BC/SRB model to add up over all the bonds
```

```
        BE+=(((BCE_i*(CN_i**0.5)/(12**0.5))/CN_i))*(bl_i/float(bl_i+bl_j))+((BCE_j*(CN_j**0.5)/(12**0.5))/CN_j)*(bl_j/float(bl_i+bl_j))

                        count+=1

    # Print out the evaluated CE of the system.

        print 'The CE = {} eV for the {} system'.format(BE/(count-2),moleculename)
```

D 1 EE_ANALYSIS FePt

```
#! /usr/bin/env python

## This script is used to calculate excess energy EE by the BC model for the FePt nanoalloy reported in

# Yang et al. Nature 2017, 542, 75-70

import sys

import numpy as np

import random

from ase.io import read,write


# Creates composition range to test

comp_Fe_Percent=np.arange(0.05,1.00,0.05)

# This factor determines how many structures are generated at the given composition

num=1000

# This is the name of the modified xyz file you are reading the cns from

moleculename = "FePt_cns_final.xyz"


Fe_surf_percent=0.4232 #42.32% of Fe atoms will be on the surface as the original


# Parameters for BC model for Fe and Pt, specifically.

bl_Fe=0.404494382

bl_Pt=1-bl_Fe

# CE values of Pure Fe/Pt MNPs at the size/shape/bonding topology of the FePt MNP
```

```
CE_Fe_pure=-3.8956485501

CE_Pt_pure=-5.31555783471



# Read name and cns from only original .xyz file

file1 = open(moleculename,'r')

lines = file1.readlines()

file1.close()

count1=0

# Construct bulk_list and surf_list that say bulk and surface atoms, respectively

surf_list=[]

bulk_list=[]

subsurf_list=[]

CNS_track=[]

neighborlist_track=[]

# Read in atomic CNs and neighborlists

# Determine bulk vs subsurface

for line in lines:

        if count1<=1:

                count1+=1

        else:

                vals=line.split()

                CN_i=float(vals[4])
```

```
            CNS_track.append(CN_i)
                w = count1-2
                vect=line.split("[") #split the line by [
            nl_i_raw=vect[1][0:-2] #pick the numbers without ]
            nl_i_raw_2=nl_i_raw.split(",") #split by ,
            nl_i = [int(i) for i in nl_i_raw_2] #convert into integer
                neighborlist_track.append(nl_i)
                if CN_i<=9:
                        surf_list.append(w)
                elif CN_i<12:
                        subsurf_list.append(w)
                else:
                        bulk_list.append(w)
                        CN_j_list=[]
                count1+=1

# Convert CNS list to numpy array
cns_track=np.asarray(CNS_track)

# Use ase to establish atomic symbols and chemical symbols
original=read(moleculename)
atomicnum=original.get_atomic_numbers()
numfes=len([x for x in atomicnum if x==26])
```

```
total=len(atomicnum)
total_list=range(total)
outsymbol=original.get_chemical_symbols()

# Define the total number of surface atoms
num_surf_atoms=len(surf_list) #atoms in subsurface and bulk

for percentfes in comp_Fe_Percent:
    x_Fe=percentfes
    x_Pt=1-percentfes
    EE_extract=x_Fe*CE_Fe_pure + x_Pt*CE_Pt_pure
    ces_structs=[]
    E_excess=[]
    for n in range(1,num+1):
        temp_BE=0
        Fe_num_total=int(23196*percentfes) #total number of atoms
        Fe_num_surf_temp=int(Fe_num_total*Fe_surf_percent) #in case Fe_surf > len(surf)
        if Fe_num_surf_temp <= 7242:
            Fe_num_surf=Fe_num_surf_temp
        else:
            Fe_num_surf=7242
        Fe_num_notsurf=Fe_num_total-Fe_num_surf #number of Fe not distributed on surface
        Fe_bulk_temp=int(Fe_num_notsurf*0.5) #in case Fe_bulk > len(bulk)
```

```
if Fe_bulk_temp <= 6931:
        Fe_num_bulk=Fe_bulk_temp
else:
        Fe_num_bulk=6931
fes=random.sample(total_list,Fe_num_total)
outvect=np.ones(total)*78
outvect[[fes]]=26
trackpt=0
trackfe=0
for i in range(total):
if outvect[i]==78.:
                outsymbol[i]='Pt'
                Ecoh_i=-5.84
                bl_i=bl_Pt
                nl_i_0=neighborlist_track[i] #neiborlist of atom i
                CN_i=cns_track[i] # CN of atom i
                for j in nl_i_0:
                        CN_j=cns_track[j] #CN of atom j
                        if outvect[j]==78.:
                                Ecoh_j=-5.84
                                bl_j=bl_Pt
                        else:
                                Ecoh_j=-4.28
```

```
                    bl_j=bl_Fe

        temp_BE+=(((Ecoh_i*(CN_i**0.5)/(12**0.5))/CN_i))*(bl_i/float(bl_i+bl_j))+((Ecoh_j*(CN_j**0.5)/(12**0.5))/CN_j)*(bl_j/float(bl_i+bl_j))
                    trackpt+=1
        else:
                    outsymbol[i]='Fe'
                    Ecoh_i=-4.28
                bl_i=bl_Fe
                nl_i_0=neighborlist_track[i] #neiborlist of atom i
                    CN_i=cns_track[i]
                for j in nl_i_0:
                        CN_j=cns_track[j]
                    if outvect[j]==78.:
                        Ecoh_j=-5.84
                        bl_j=bl_Pt
                    else:
                        Ecoh_j=-4.28
                        bl_j=bl_Fe

temp_BE+=(((Ecoh_i*(CN_i**0.5)/(12**0.5))/CN_i))*(bl_i/float(bl_i+bl_j))+((Ecoh_j*(CN_j**0.5)/(12**0.5))/CN_j)*(bl_j/float(bl_i+bl_j))
                    trackfe+=1
        ces_structs.append(temp_BE/total)
```

```
        CE=temp_BE/total
        E_e=CE-EE_extract
        E_excess.append(E_e)

# Write out only the CEs for each of the generated structures
    file3=open('{}_surf_CE.txt'.format(int(percentfes*100)),'w')
    for j in ces_structs:
        file3.write('{}\n'.format(j))
    file3.close()
    file4=open('{}_ExcessE.txt'.format(int(percentfes*100)),'w')
    for m in E_excess:
        file4.write('{}\n'.format(m))
    file4.close()
```

BIBLIOGRAPHY

1. Kittel, C., Introduction to Solid State Physics. *American Journal of Physics* **2004,** *35*, 547.

2. Morse, M. D., Clusters of transition-metal atoms. *Chem. Rev.* **1986,** *86* (6), 1049-1109.

3. Yang, Y.; Chen, C.-C.; Scott, M. C.; Ophus, C.; Xu, R.; Pryor, A.; Wu, L.; Sun, F.; Theis, W.; Zhou, J.; Eisenbach, M.; Kent, P. R. C.; Sabirianov, R. F.; Zeng, H.; Ercius, P.; Miao, J., Deciphering chemical order/disorder and material properties at the single-atom level. *Nature* **2017,** *542* (7639), 75-79.

4. Talapin, D. V.; Lee, J. S.; Kovalenko, M. V.; Shevchenko, E. V., Prospects of Colloidal Nanocrystals for Electronic and Optoelectronic Applications. *Chem. Rev.* **2010,** *110* (1), 389-458.

5. De, M.; Ghosh, P. S.; Rotello, V. M., Applications of Nanoparticles in Biology. *Adv. Mater.* **2008,** *20* (22), 4225-4241.

6. Ferrando, R.; Jellinek, J.; Johnston, R. L., Nanoalloys: From theory to applications of alloy clusters and nanoparticles. *Chem. Rev.* **2008,** *108* (3), 845-910.

7. Haruta, M.; Kobayashi, T.; Sano, H.; Yamada, N., Novel Gold Catalysts for the Oxidation of Carbon Monoxide at a Temperature far Below 0 °C. *Chem. Lett.* **1987,** (2), 405-408.

8. Kelly, K. L.; Coronado, E.; Zhao, L. L.; Schatz, G. C., The optical properties of metal nanoparticles: The influence of size, shape, and dielectric environment. *J. Phys. Chem. B* **2003,** *107* (3), 668-677.

9. Yan, Y.; Warren, S. C.; Fuller, P.; Grzybowski, B. A., Chemoelectronic circuits based on metal nanoparticles. *Nat. Nanotechnol.* **2016,** *11* (7), 603-608.

10. Wessels, J. M.; Nothofer, H.-G.; Ford, W. E.; von Wrochem, F.; Scholz, F.; Vossmeyer, T.; Schroedter, A.; Weller, H.; Yasuda, A., Optical and Electrical Properties of Three-Dimensional Interlinked Gold Nanoparticle Assemblies. *Journal of the American Chemical Society* **2004,** *126* (10), 3349-3356.

11. Duan, S. B.; Wang, R. M., Bimetallic nanostructures with magnetic and noble metals and their physicochemical applications. *Prog. Nat. Sci.* **2013,** *23* (2), 113-126.

12. Cuenya, B. R., Synthesis and catalytic properties of metal nanoparticles: Size, shape, support, composition, and oxidation state effects. *Thin Solid Films* **2010,** *518* (12), 3127-3150.

13. Bell, A. T., The impact of nanoscience on heterogeneous catalysis. *Science* **2003,** *299* (5613), 1688-1691.

14. Mpourmpakis, G.; Andriotis, A. N.; Vlachos, D. G., Identification of Descriptors for the CO Interaction with Metal Nanoparticles. *Nano Lett.* **2010,** *10* (3), 1041-1045.

15. Taylor, M. G.; Austin, N.; Gounaris, C. E.; Mpourmpakis, G., Catalyst Design Based on Morphology- and Environment-Dependent Adsorption on Metal Nanoparticles. *ACS Catalysis* **2015,** *5* (11), 6296-6301.

16. Hoare, M. R.; Pal, P., Geometry and Stability of "Spherical" f.c.c. Microcrystallites. *Nature Physical Science* **1972,** *236*, 35.

17. Bratlie, K. M.; Lee, H.; Komvopoulos, K.; Yang, P. D.; Somorjai, G. A., Platinum nanoparticle shape effects on benzene hydrogenation selectivity. *Nano Lett.* **2007,** *7* (10), 3097-3101.

18. Luo, L.; Duan, Z.; Li, H.; Kim, J.; Henkelman, G.; Crooks, R. M., Tunability of the Adsorbate Binding on Bimetallic Alloy Nanoparticles for the Optimization of Catalytic Hydrogenation. *Journal of the American Chemical Society* **2017,** *139* (15), 5538-5546.

19. Jiang, H.-L.; Akita, T.; Ishida, T.; Haruta, M.; Xu, Q., Synergistic Catalysis of Au@Ag Core−Shell Nanoparticles Stabilized on Metal−Organic Framework. *Journal of the American Chemical Society* **2011,** *133* (5), 1304-1306.

20. Link, S.; Burda, C.; Wang, Z. L.; El-Sayed, M. A., Electron dynamics in gold and gold–silver alloy nanoparticles: The influence of a nonequilibrium electron distribution and the size dependence of the electron–phonon relaxation. *The Journal of Chemical Physics* **1999,** *111* (3), 1255-1264.

21. Yang, Y. S.; Chen, C. C.; Scott, M. C.; Ophus, C.; Xu, R.; Pryor, A.; Wu, L.; Sun, F.; Theis, W.; Zhou, J. H.; Eisenbach, M.; Kent, P. R. C.; Sabirianov, R. F.; Zeng, H.; Ercius, P.; Miao, J. W., Deciphering chemical order/disorder and material properties at the single-atom level. *Nature* **2017,** *542* (7639), 75-79.

22. Yudanov, I. V.; Genest, A.; Schauermann, S.; Freund, H. J.; Rosch, N., Size Dependence of the Adsorption Energy of CO on Metal Nanoparticles: A DFT Search for the Minimum Value. *Nano Lett.* **2012,** *12* (4), 2134-2139.

23. Daw, M. S.; Baskes, M. I., Embedded-atom method: Derivation and application to impurities, surfaces, and other defects in metals. *Physical Review B* **1984,** *29* (12), 6443-6453.

24. Daw, M. S.; Foiles, S. M.; Baskes, M. I., The embedded-atom method: a review of theory and applications. *Materials Science Reports* **1993,** *9* (7-8), 251-310.

25. Kohn, W., Electronic structure of matter: Wave functions and density functionals. *Chimia* **2000,** *54* (1-2), 50-50.

26. Haberlen, O. D.; Chung, S. C.; Stener, M.; Rosch, N., From clusters to bulk: A relativistic density functional investigation on a series of gold clusters Au-n, n=6, ..., 147. *Journal of Chemical Physics* **1997,** *106* (12), 5189-5201.

27. Cleri, F.; Rosato, V., Tight-binding potentials for transition metals and alloys. *Physical Review B* **1993,** *48* (1), 22-33.

28. Rosato, V.; Guillope, M.; Legrand, B., Thermodynamical and structural properties of f.c.c. transition metals using a simple tight-binding model. *Philosophical Magazine A* **1989,** *59* (2), 321-336.

29. Tomanek, D.; Mukherjee, S.; Bennemann, K. H., Simple theory for the electronic and atomic structure of small clusters. *Physical Review B* **1983,** *28* (2), 665-673.

30. Kohn, W.; Sham, L. J., Self-Consistent Equations Including Exchange and Correlation Effects. *Physical Review* **1965,** *140* (4A), 1133-&.

31. Jones, R. O., Density functional theory: Its origins, rise to prominence, and future. *Reviews of Modern Physics* **2015,** *87* (3), 897-923.

32. Hafner, J.; Wolverton, C.; Ceder, G., Toward Computational Materials Design: The Impact of Density Functional Theory on Materials Research. *MRS Bulletin* **2011,** *31* (9), 659-668.

33. Schrödinger, E., An Undulatory Theory of the Mechanics of Atoms and Molecules. *Physical Review* **1926,** *28* (6), 1049-1070.

34. Perdew, J. P.; Chevary, J. A.; Vosko, S. H.; Jackson, K. A.; Pederson, M. R.; Singh, D. J.; Fiolhais, C., Atoms, molecules, solids, and surfaces: Applications of the generalized gradient approximation for exchange and correlation. *Physical Review B* **1992,** *46* (11), 6671-6687.

35. Langreth, D. C.; Mehl, M. J., Beyond the local-density approximation in calculations of ground-state electronic properties. *Physical Review B* **1983,** *28* (4), 1809-1834.

36. Li, Y.; Galli, G.; Gygi, F., Electronic Structure of Thiolate-Covered Gold Nanoparticles: Au102(MBA)44. *ACS Nano* **2008,** *2* (9), 1896-1902.

37. Aikens, C. M., Electronic Structure of Ligand-Passivated Gold and Silver Nanoclusters. *The Journal of Physical Chemistry Letters* **2011,** *2* (2), 99-104.

38. Ernzerhof, M.; Scuseria, G. E., Assessment of the Perdew-Burke-Ernzerhof exchange-correlation functional. *Journal of Chemical Physics* **1999,** *110* (11), 5029-5036.

39. Yoon, Y.; Rousseau, R.; Weber, R. S.; Mei, D. H.; Lercher, J. A., First-Principles Study of Phenol Hydrogenation on Pt and Ni Catalysts in Aqueous Phase. *Journal of the American Chemical Society* **2014,** *136* (29), 10287-10298.

40. Wang, Y. G.; Mei, D. H.; Glezakou, V. A.; Li, J.; Rousseau, R., Dynamic formation of single-atom catalytic active sites on ceria-supported gold nanoparticles. *Nat. Commun.* **2015,** *6*, 8.

41. Aarons, J.; Sarwar, M.; Thompsett, D.; Skylaris, C. K., Perspective: Methods for large-scale density functional calculations on metallic systems. *Journal of Chemical Physics* **2016,** *145* (22).

42. Wang, D. L.; Xin, H. L. L.; Hovden, R.; Wang, H. S.; Yu, Y. C.; Muller, D. A.; DiSalvo, F. J.; Abruna, H. D., Structurally ordered intermetallic platinum-cobalt core-shell nanoparticles with enhanced activity and stability as oxygen reduction electrocatalysts. *Nature Materials* **2013,** *12* (1), 81-87.

43. Kozlov, S. M.; Kovacs, G.; Ferrando, R.; Neyman, K. M., How to determine accurate chemical ordering in several nanometer large bimetallic crystallites from electronic structure calculations. *Chemical Science* **2015,** *6* (7), 3868-3880.

44. Sutton, A. P.; Finnis, M. W.; Pettifor, D. G.; Ohta, Y., THE TIGHT-BINDING BOND MODEL. *Journal of Physics C-Solid State Physics* **1988,** *21* (1), 35-66.

45. Ducastelle, F., Modules élastiques des métaux de transition. *Journal de Physique* **1970,** *31* (11-12), 1055-1062.

46. Tomanek, D.; Aligia, A. A.; Balseiro, C. A., Calculation of elastic strain and electronic effects on surface segregation. *Physical Review B* **1985,** *32* (8), 5051-5056.

47. Ackland, G. J.; Finnis, M. W.; Vitek, V., Validity of the second moment tight-binding model. *Journal of Physics F: Metal Physics* **1988,** *18* (8), L153.

48. Kittel, C., Introduction to Solid State Physics. *8th edition. Hoboken, NJ: John Wiley & Sons, Inc* **2005**, 50.

49. Perdew, J. P.; Burke, K.; Ernzerhof, M., Generalized gradient approximation made simple. *Phys. Rev. Lett.* **1996,** *77* (18), 3865-3868.

50. Godbout, N.; Salahub, D. R.; Andzelm, J.; Wimmer, E., Optimization of Gaussian-type basis sets for local spin density functional calculations. Part I. Boron through neon, optimization technique and validation. *Canadian Journal of Chemistry* **1992,** *70* (2), 560-571.

51. Hutter, J.; Iannuzzi, M.; Schiffmann, F.; VandeVondele, J., CP2K: atomistic simulations of condensed matter systems. *Wiley Interdiscip. Rev.-Comput. Mol. Sci.* **2014,** *4* (1), 15-25.

52. Yan, Z.; Taylor, M. G.; Mascareno, A.; Mpourmpakis, G., Size-, Shape-, and Composition-Dependent Model for Metal Nanoparticle Stability Prediction. *Nano Lett.* **2018,** *18* (4), 2696-2704.

53. Hu, S. Z.; Zhou, Z. H.; Robertson, B. E., Consistent approaches to van der Waals radii for the metallic elements. *Zeitschrift Fur Kristallographie* **2009,** *224* (8), 375-383.

54. Austin, N.; Ye, J.; Mpourmpakis, G., CO2 activation on Cu-based Zr-decorated nanoparticles. *Catal. Sci. Technol.* **2017,** *7* (11), 2245-2251.

55. Janthon, P.; Luo, S. J.; Kozlov, S. M.; Vines, F.; Limtrakul, J.; Truhlar, D. G.; Illas, F., Bulk Properties of Transition Metals: A Challenge for the Design of Universal Density Functionals. *Journal of Chemical Theory and Computation* **2014,** *10* (9), 3832-3839.

56. Eberhart, J. G.; Horner, S., Bond-Energy and Surface-Energy Calculations in Metals. *Journal of Chemical Education* **2010,** *87* (6), 608-612.

57. Finnis, M. W.; Sinclair, J. E., A simple empirical N-body potential for transition metals. *Philosophical Magazine A* **1984,** *50* (1), 45-55.

58. Li, H.; Li, L.; Pedersen, A.; Gao, Y.; Khetrapal, N.; Jonsson, H.; Zeng, X. C., Magic-Number Gold Nanoclusters with Diameters from 1 to 3.5 nm: Relative Stability and Catalytic Activity for CO Oxidation. *Nano Lett.* **2015,** *15* (1), 682-688.

59. Wang, H. L.; Zhou, S.; Gilroy, K. D.; Cai, Z. S.; Xia, Y. N., Icosahedral nanocrystals of noble metals: Synthesis and applications. *Nano Today* **2017,** *15*, 121-144.

60. Linic, S.; Christopher, P.; Ingram, D. B., Plasmonic-metal nanostructures for efficient conversion of solar to chemical energy. *Nature Materials* **2011,** *10* (12), 911-921.

61. Guedes-Sobrinho, D.; Nomiyama, R. K.; Chaves, A. S.; Piotrowski, M. J.; Da Silva, J. L. F., Structure, Electronic, and Magnetic Properties of Binary Pt_nTM_{55-n} (TM = Fe, Co, Ni, Cu, Zn) Nanoclusters: A Density Functional Theory Investigation. *Journal of Physical Chemistry C* **2015,** *119* (27), 15669-15679.

62. McDavid, J. M.; Fain, S. C., Segregation at Cu Au alloy surfaces. *Surface Science* **1975,** *52* (1), 161-173.